

Research Article

The Eaf3 chromodomain acts as a pH sensor for gene expression by altering its binding affinity for histone methylated-lysine residues

 Masahiko Okuda and  Yoshifumi Nishimura

Graduate School of Medical Life Science, Yokohama City University, 1-7-29 Suehiro-cho, Tsurumi-ku, Yokohama 230-0045, Japan

Correspondence: Yoshifumi Nishimura (nisimura@yokohama-cu.ac.jp)



During gene expression, histone acetylation by histone acetyltransferase (HAT) loosens the chromatin structure around the promoter to allow RNA polymerase II (Pol II) to initiate transcription, while de-acetylation by histone deacetylase (HDAC) tightens the structure in the transcribing region to repress false initiation. Histone acetylation is also regulated by intracellular pH (pH_i) with global hypoacetylation observed at low pH_i , and hyperacetylation, causing proliferation, observed at high pH_i . However, the mechanism underlying the pH_i -dependent regulation of gene expression remains elusive. Here, we have explored the role of the chromodomain (CD) of budding yeast Eaf3, a common subunit of both HAT and HDAC that is thought to recognize methylated lysine residues on histone H3. We found that Eaf3 CD interacts with histone H3 peptides methylated at Lys4 (H3K4me, a promoter epigenetic marker) and Lys36 (H3K36me, a coding region epigenetic marker), as well as with many dimethyl-lysine peptides and even arginine-asymmetrically dimethylated peptides, but not with unmethylated, phosphorylated or acetylated peptides. The Eaf3 CD structure revealed an unexpected histidine residue in the aromatic cage essential for binding H3K4me and H3K36me. pH titration experiments showed that protonation of the histidine residue around physiological pH controls the charge state of the aromatic cage to regulate binding to H3K4me and H3K36me. Histidine substitution and NMR experiments confirmed the correlation of histidine pK_a with binding affinity. Collectively, our findings suggest that Eaf3 CD functions as a pH_i sensor and a regulator of gene expression via its pH_i -dependent interaction with methylated nucleosomes.

Introduction

Post-translational modifications of histones play an essential role in the regulation of transcription, DNA repair, replication and heterochromatin formation by changing the chromatin structure. For example, histones are specifically acetylated and methylated to induce gene expression [1,2]. *Saccharomyces cerevisiae* shows a global pattern of histone H3 and H4 acetylation, whereby acetylation is higher at promoters and lower in coding regions [3,4]. Acetylation loosens the chromatin structure, allowing RNA polymerase II (Pol II) to easily access the promoter; in transcribing regions, by contrast, de-acetylation tightens the chromatin structure, meaning that Pol II can read the gene information but cannot access the gene to start transcription from a cryptic site. Similar to these patterns of acetylation, lysine 4 of histone H3 (H3K4) is methylated by Set1 methyltransferase at promoter sites, whereas Set2 methyltransferase mediates H3K36 methylation in coding regions [5].

In addition to the acetylation pattern for gene expression, histone acetylation is also affected by intracellular pH (pH_i) in both normal and cancer cells [6]. When pH_i decreases, histones are globally

Received: 10 June 2019
Revised: 31 January 2020
Accepted: 05 February 2020

Accepted Manuscript online:
07 February 2020
Version of Record published:
20 February 2020

de-acetylated by histone deacetylases (HDACs), and the released acetate anions are co-exported with protons from cells by monocarboxylate transporters to maintain pH_i . Further decreases in pH_i have been shown to trigger apoptosis [7]. Alongside the rising pH_i that occurs when resting cells are induced to proliferate, differentiate and progress in the cell cycle [8], global acetylation of histone increases.

Although an apparent relation between pH_i and histone acetylation responsible for gene expression has been reported, the pH_i -dependent molecular mechanism of gene expression due to histone acetylation and methylation remains elusive. In terms of the relation between acetylation and methylation, Eaf3 (essential Sas2-related acetyltransferase1-associated factor 3) is a key protein in *S. cerevisiae*. Eaf3 is a component of both the NuA4 histone acetyltransferase (HAT) complex and the Rpd3S HDAC complex. It is thought that the N-terminal chromodomain (CD) of Eaf3 recognizes H3K36 methylation, which then positions Rpd3S on the nucleosome to suppress intragenic transcription initiation [9–11]. However, binding between Eaf3 CD and methylated H3K36 (H3K36me) is relatively weak; therefore, it is thought that Eaf3 CD determines the specificity for H3K36me but the strong binding affinity is cooperatively mediated by the Rco1 subunit of Rpd3S via its plant homeodomain (PHD) [12,13]. Because of the weak interaction, the structure of Eaf3 CD bound to the H3K36me peptide was determined by NMR using a fusion protein of the CD and a model H3K36me peptide [14].

Notably, Eaf3 is also a subunit of the NuA4 HAT complex, which recognizes H3K4me at promoter site nucleosomes. In fact, Eaf3 CD can also bind weakly to H3K4me, facilitating recruitment of NuA4 to the promoter region. Similar to Rpd3S, the PHD of the Yng2 subunit of NuA4 plays an essential cooperative role in binding of Eaf3 CD to H3K4me [15,16]. Thus, Eaf3 CD seems to have no strong sequence specificity and can bind to both H3K4me and H3K36me, while the specific recruitment of NuA4 and Rpd3S to H3K4me and H3K36me, respectively, is cooperatively determined by the PHD of the respective Yng2 and Rco1 subunits. Nevertheless, the cooperative effect of Eaf3 is important because cells lacking Eaf3 have an even distribution of histone acetylation levels across the genome, whereas wild-type (WT) cells have higher histone acetylation levels at promoter regions than at coding sequences [17].

Here, we have explored the role of Eaf3 CD binding to H3K4me and H3K36me. We examined the complexes of Eaf3 CD bound to lysine-methylated histones, which showed that Eaf3 CD is a unique module containing a histidine, His18, in its binding pocket for methylated lysine residues of histones, even though a positively charged residue would be expected to repulse the positively charged histone methyl-lysine. Protonation of His18 was found to critically control both the binding activity and the pH sensitivity of Eaf3 CD: at high pH_i , the deprotonation of Eaf3 CD causes strong binding to H3K4me at promoters via NuA4, and to H3K36me at transcribing regions via Rpd3S. Thus, the role of Eaf3 CD is to act as a sensor of pH_i to control gene expression, rather than to act as a determinant of binding between H3K4me and H3K36me, which is achieved by other components in NuA4 and Rpd3S.

Materials and methods

Purification of Eaf3 CD

WT and mutants of Eaf3 CD (residues 1–120) were expressed as hexa-histidine-tagged products in pET15b vectors (Novagen) in *Escherichia coli* BL21(DE3)pLysS (Novagen). Lysed supernatant was loaded onto a Ni-nitrilotriacetic acid (NTA)-agarose (Qiagen) column. Eluted His-tagged Eaf3 CD was then treated with thrombin to remove the 6xHis-tag. The sample was again loaded onto the Ni-NTA agarose column. Fractions passing through the column were concentrated and applied onto Superdex75 (GE Healthcare).

Chemical shift perturbation

Histone H3 and H4 peptides were synthesized and purchased from Qiagen and SIGMA Genosys. The histone peptide was added to 0.1 mM ^{15}N -labeled Eaf3 CD at a molar ratio of 1:4, or 1:8, or 1:16 (Eaf3:histone) in 10 mM potassium phosphate (pH 6.8), 20 mM NaCl, and 5 mM deuterated DTT dissolved in 90% $\text{H}_2\text{O}/10\% \text{D}_2\text{O}$. ^1H , ^{15}N -HSQC spectra were acquired before and after peptide addition at 25°C on a Bruker AVANCE-600 spectrometer equipped with a cryogenic probe. Chemical shift change was calculated as $\Delta\delta = \{(\Delta\delta^1\text{H})^2 + (\Delta\delta^{15}\text{N}/5)^2\}^{1/2}$.

Peptide titration

For titration, 0.1 mM ^{15}N -labeled WT or mutant Eaf3 CD (protein) was titrated with increasing amounts of unlabeled histone H3 peptide, trimethylated lysine, or asymmetrically dimethylated arginine (ligand) in 10 mM potassium phosphate (pH 6.8), 20 mM NaCl, and 5 mM deuterated DTT dissolved in 90% $\text{H}_2\text{O}/10\% \text{D}_2\text{O}$ at 25°C on a Bruker AVANCE-600 spectrometer equipped with a cryogenic probe. In the experiments using H3K36me3 peptide at different pH, the titration was performed in 10 mM sodium acetate at pH 5.2; 10 mM potassium phosphate at

pH 6.0 or 7.5; or 10 mM Tris containing 20 mM NaCl at pH 8.5. NMR signal changes were measured by recording ^1H , ^{15}N -HSQC spectra before and after each addition. Where an interaction was detected, the ligand was added at a molar ratio of 1:4, 1:8, 1:12, 1:16, 1:20, 1:24, 1:28, 1:40, 1:52, 1:64 and 1:88, where no interaction was observed, ligand was added at 1:8, 1:16, 1:28, 1:40, 1:52, 1:64 and 1:88. Chemical shift change $\Delta\delta$ was computed by using the formula $\Delta\delta = \{(\Delta\delta^1\text{H})^2 + (\Delta\delta^{15}\text{N}/5)^2\}^{1/2}$ and plotted as a function of molar ratio. K_d values were calculated by employing the following nonlinear regression fitting function:

$$\Delta\delta = \Delta\delta_{\max} \left(K_d + [P]_t + [L]_t - \left\{ (K_d + [P]_t + [L]_t)^2 - 4[P]_t[L]_t \right\}^{1/2} \right) / 2[P]_t$$

where $\Delta\delta_{\max}$ is the maximal change in chemical shift, and $[P]_t$ and $[L]_t$ are the total concentrations of protein and ligand, respectively.

NMR structure determination

For the structure determination, 1.0–1.5 mM Eaf3 CD in 10 mM potassium phosphate (pH 6.8), 20 mM NaCl and 5 mM deuterated DTT dissolved in either 90% $\text{H}_2\text{O}/10\%$ D_2O or 99.9% D_2O was used. NMR experiments were performed at 25°C on a Bruker AVANCE-500, AVANCE-600 or AVANCE-800 spectrometer equipped with a cryogenic probe. Backbone and side chain resonances were assigned by using CBCA(CO)NH, CBCANH, HN(CO)CA, HNCA, HN(CA)CO, HNCO, HBHA(CO)NH, HCCH-COSY, HCCH-TOCSY, CCCONH and HCCCONH [18]. Aromatic side chain resonances were assigned by using DQF-COSY, TOCSY, (HB)CB(CGCD)HD, (HB)CB(CGCDCE)HE [19], CG(CB)H, CG(CD)H and CG(CDCE)H [20]. Stereospecific assignments were obtained from a combination of HNHB, HN(CO)HB, HNCG, HN(CO)CG [21] and ^{13}C -edited NOESY-HSQC ($\tau_m = 50$ ms) [18]. Distance restraints were obtained from NOESY, ^{15}N -edited NOESY-HSQC ($\tau_m = 150$ ms) and ^{13}C -edited NOESY-HSQC ($\tau_m = 50$ and 100 ms). Side-chain torsion angles, χ_1 and χ_2 , were obtained from a combination of HNHB, HN(CO)HB, HNCG, HN(CO)CG [21] and ^{13}C -edited NOESY-HSQC ($\tau_m = 50$ ms) [18]. Hydrogen bond restraints were obtained by backbone amide H/D-exchange experiments. Spectra were processed by NMRPipe [22] and analyzed by NMRView [23].

Structure calculation

Interproton distance restraints derived from NOE intensities were grouped into four distance ranges, 1.8–2.7 Å (1.8–2.9 Å for NOEs involving HN protons), 1.8–3.3 Å (1.8–3.5 Å for NOEs involving HN protons), 1.8–5.0 Å and 1.8–6.0 Å, corresponding to strong, medium, weak and very weak NOEs, respectively. The upper limit was corrected for constraints involving methyl groups, aromatic ring protons and non-stereospecifically assigned methylene protons. Dihedral angle restraints for ϕ and ψ were obtained by analyzing the backbone chemical shifts with TALOS [24]. χ_1 and χ_2 angles were restrained $\pm 30^\circ$ for three side-chain rotamers. Structure calculations were performed by distance geometry and simulated annealing by using Xplor-NIH [25,26], and all structures were subjected to water refinement [27]. A total of 200 structures were calculated. Structural statistics for the 20 best structures are summarized in Supplementary Table S2. Structures were analyzed and displayed using PROCHECK-NMR [28], MOLMOL [29] and PyMOL (Schroedinger).

NMR relaxation analysis

The order parameter, S^2 , was obtained from the model-free analysis assuming axially symmetric rotation. The backbone ^{15}N relaxation parameters of Eaf3 CD were measured by using a ^{15}N -labeled sample of 0.30 mM at 25°C on a Bruker AVANCE-600 (^{15}N frequency, 60.8 MHz) spectrometer equipped with a cryogenic probe. Relaxation durations of 24, 256, 512, 768, 1024, 1280, 1536, 2048 and 2560 ms for the longitudinal relaxation rates (R_1), and 16.98, 33.95, 50.93, 67.90, 101.86, 135.81, 203.71 and 339.52 ms for the transverse relaxation rates (R_2) were used. Heteronuclear ^{15}N - $\{^1\text{H}\}$ NOE experiments were recorded in the presence and absence of proton saturation, which was achieved with a 5.0 s duration consisting of 120° ^1H pulses applied every 5.0 ms. R_1 and R_2 were obtained by fitting peak intensities at a series of relaxation durations to an exponential decay curve using CurveFit [30]. The uncertainties of the peak intensities were estimated by using duplicated data from the shortest relaxation delay. The uncertainties of the relaxation rates were determined by CurveFit using a Monte–Carlo simulation. The steady-state ^{15}N - $\{^1\text{H}\}$ NOE values were determined from peak intensity ratios obtained from spectra acquired with and without proton saturation. The uncertainties were determined from the standard deviation in background noise levels by using NMRView [23]. Initial values of the overall correlation time and the axially symmetric rotational diffusion tensor were estimated by using r2r1_diffusion [31]. Model-free analysis was performed by using Modelfree [30] and FAST ModelFree [32].

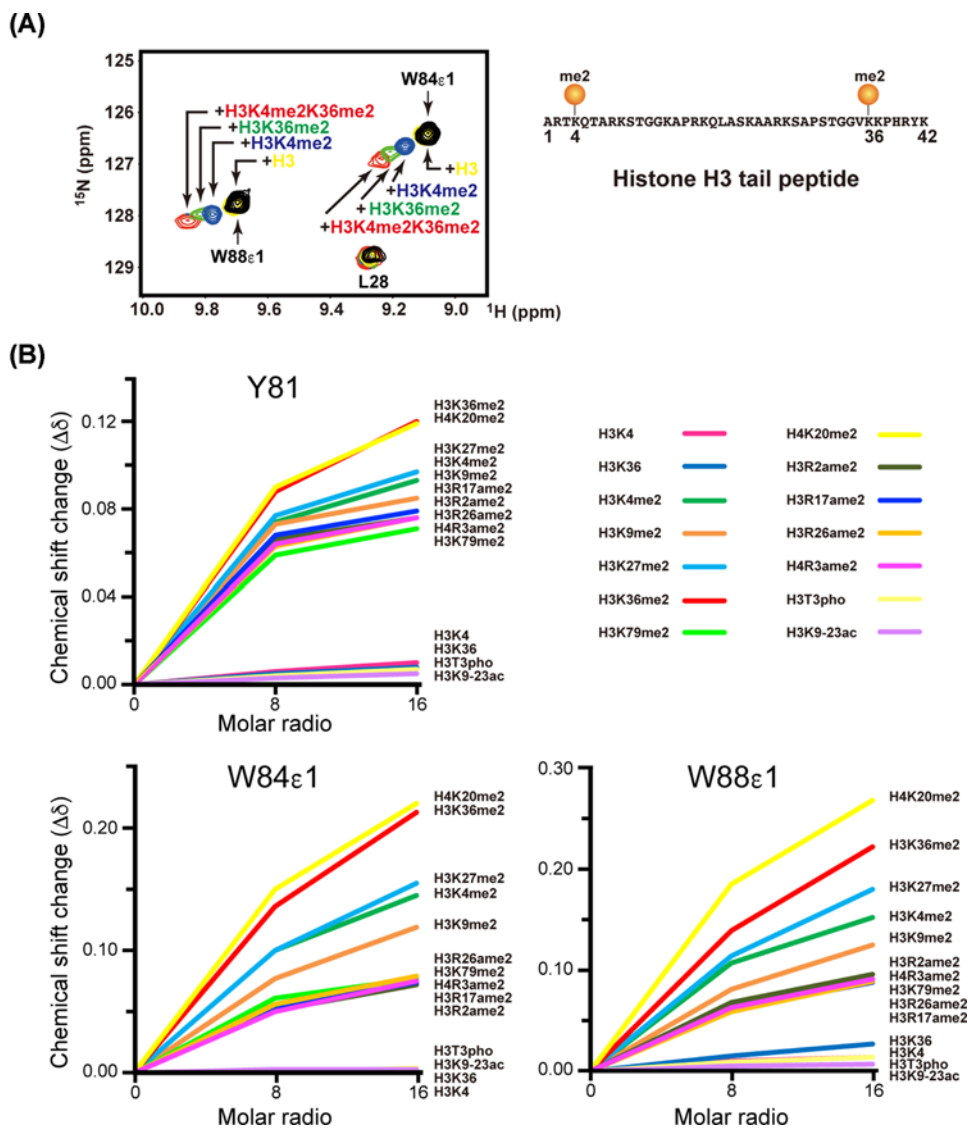


Figure 1. Perturbation of the NMR chemical shift of Eaf3 CD by various post-translationally modified histone peptides
(A) Overlays of an expanded region of the $^1\text{H},^{15}\text{N}$ -HSQC spectrum of Eaf3 CD before (black) and after the addition of a 4-fold excess of histone H3 peptide (residues 1-42): H3 (yellow), H3K4me2 (blue), H3K36me2 (green) and H3K4me2K36me2 (red). me2: di-methylated. **(B)** Chemical shift change ($\Delta\delta$) of the backbone amide group of Tyr81 and side-chain imino groups of Trp84 and Trp88 at a molar ratio of 1:8 and 1:16. The added histone peptides are shown on the right. ame2: asymmetrically di-methylated, pho: phosphorylated, ac: acetylated.

pH titration

A series of $^1\text{H},^{15}\text{N}$ -HSQC spectra for 0.1–1.1 mM ^{15}N -labeled Eaf3 CD were recorded at different pH ranging from 5.2 to 10.5 at 25°C on a Bruker AVANCE-600 spectrometer equipped with a cryogenic probe. The observed chemical shift (δ_{obs}) was plotted as a function of pH. pK_a values were calculated by a nonlinear least-squares fit of the pH titration curves using the following equation,

$$\delta_{\text{obs}} = \frac{[\delta_l + \delta_h \times 10^{(\text{pH}-pK_a)}]}{[1 + 10^{(\text{pH}-pK_a)}]}$$

where δ_l and δ_h represent the chemical shift values at extreme low and high pH, respectively.

Table 1 Dissociation constant (K_d) for binding of Eaf3 CD to histone H3 peptide

Histone	K_d (μ M)
Kme3*	4440 \pm 230
H3K36	N.B.
H3K36me2	3350 \pm 200
H3K36me3	1880 \pm 130
H3K4	N.B.
H3K4me2	4040 \pm 110
H3K4me3	2900 \pm 10
H3R2ame2K4me3	1360 \pm 20
H3T3phoK3me3	6520 \pm 480
Rame2*	>10,000

* amino acid, N.B.: not bound.

PRE

A 4-fold molar excess of the spin label reagent MTSL (1-oxy-2,2,5,5-tetramethyl-D3-pyrroline-3-methyl) methanethiosulfonate (Toronto Research Chemicals) dissolved in acetonitrile was added to H3K36me3 peptide (residues 32–41) with a Gly33Cys substitution (SIGMA Genosys), dissolved in buffer [10 mM potassium phosphate (pH 6.8), 20 mM NaCl], and incubated at 25°C for 16 h in the dark. Unreacted MTSL was removed by using a PD MidiTrap G-10 column (GE Healthcare) equilibrated with distilled water. The spin labeled peptide eluted with water was lyophilized and dissolved in buffer, and the pH was adjusted to 6.8. A paramagnetic sample was obtained by adding MTSL-H3K36me3 peptide to 15 N-labeled Eaf3 CD dissolved in buffer at a molar ratio of 1:1 (final concentration 0.3 mM), and the ^1H , ^{15}N -HSQC spectrum was recorded. A diamagnetic sample was generated by reducing the paramagnetic sample with a 3.2-fold molar excess of ascorbate (Wako) at 25°C for 4 h in the dark. After the reduction, the ^1H , ^{15}N -HSQC spectrum was recorded.

Results

Methyl-specific binding of Eaf3 CD

It has been reported that Eaf3 CD binds weakly to the H3K4me peptide as well as the H3K36me peptide [9,10,14,33]. To confirm this, we monitored NMR signal changes of ^{15}N -labeled Eaf3 CD upon the addition of histone peptides by using ^1H , ^{15}N HSQC spectroscopy. Initially, we examined the methylation-dependent specificity of binding to the N-terminal fragment (residues 1–42) of histone H3 (H3) (Figure 1A and Supplementary Table S1). The addition of a 4-fold excess of an H3 peptide di-methylated (me2) at K4, K36, or both lysine residues gave rise to a small but significant signal change of specific residues such as Tyr81, Trp84 and Trp88, which formed a binding pocket (Supplementary Figure S1a). By contrast, the addition of a 4-fold excess of unmodified H3 peptide did not result in any altered signals.

To characterize the weak binding of Eaf3 CD in more detail, we observed the interaction of Eaf3 CD with various histone peptides (Figure 1B and Supplementary Table S1). Eaf3 CD interacted with many dimethyl-lysine peptides, and even with arginine-asymmetrically dimethylated (ame2) peptides, but not with unmethylated, phosphorylated (pho) or acetylated (ac) peptides. Thus, the binding of Eaf3 CD to histone is highly methylation-specific but promiscuous.

Eaf3 CD binds preferentially to trimethylated peptides and to H3K36me2/3

Because the NuA4 and Rpd3S complexes are closely related to H3K4me and H3K36me, respectively, we focused on these methylation marks and evaluated their quantitative binding to Eaf3 CD by NMR titration (Table 1 and Figure 2). We found that Eaf3 CD bound more strongly (i) to the trimethylated form than to the dimethylated form of both H3K4 and H3K36 and (ii) to di- and trimethylated H3K36 than to the corresponding methylated forms of H3K4. In addition, binding to H3K4me3 was strengthened by R2ame2 modification, but weakened by T3pho modification. Although the different binding features observed were interesting, in all cases the dissociation constant (K_d) values were in the millimolar range. Thus, Eaf3 CD can be categorized as a very weak histone methyl-lysine-binding module.

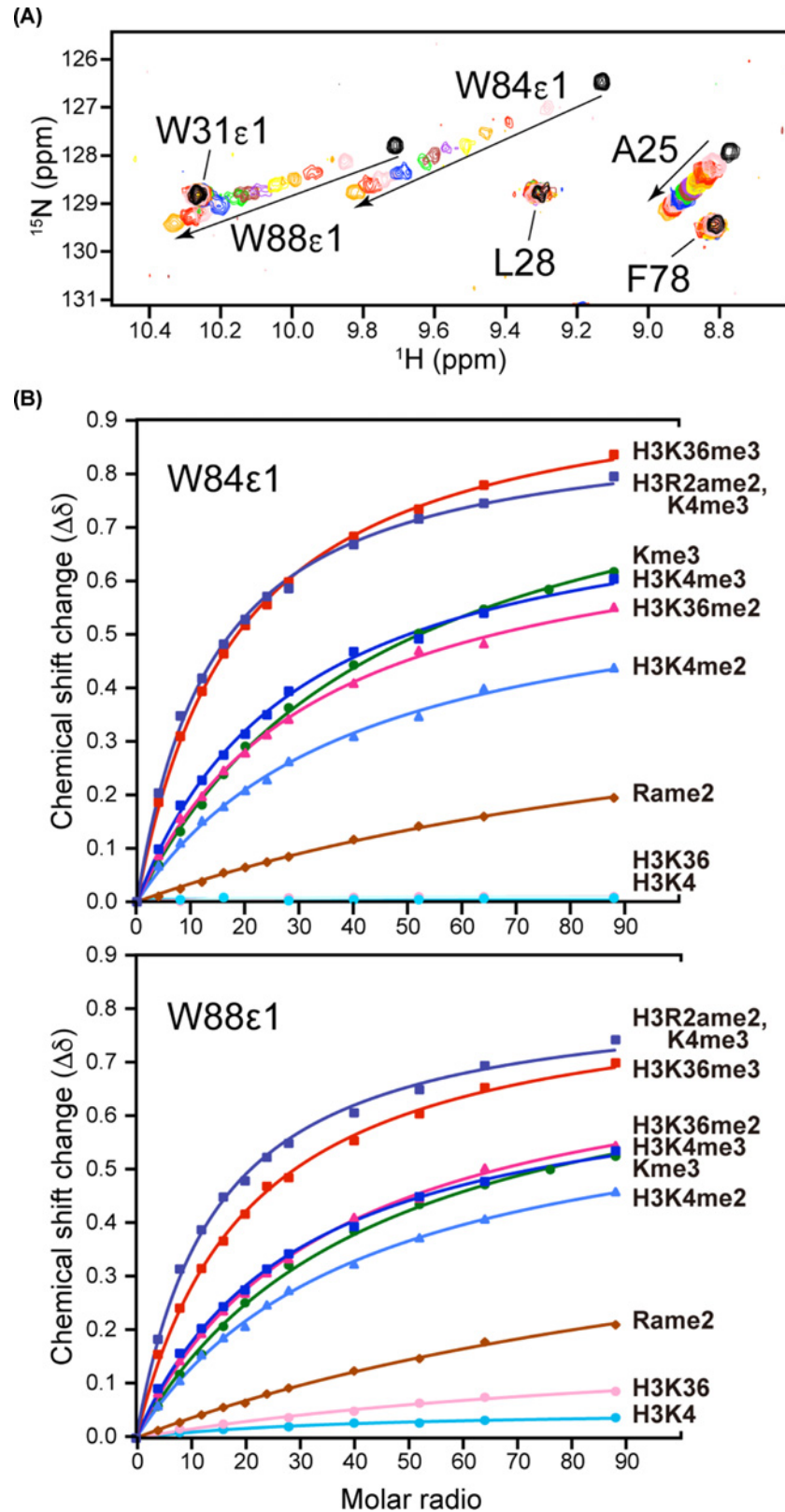


Figure 2. NMR titration of Eaf3 CD with K4- or K36-methylated histone H3 peptide

(A) Overlays of an expanded region of the ^1H , ^{15}N -HSQC spectrum of Eaf3 CD titrated with H3K36me3 peptide. (B) Titration curves for the side chain imino groups from Trp84 and Trp88 of Eaf3 CD. The added histone peptides and amino acids are shown on the right. Kme3: tri-methyl-lysine, Rame2: asymmetrically di-methylated arginine.

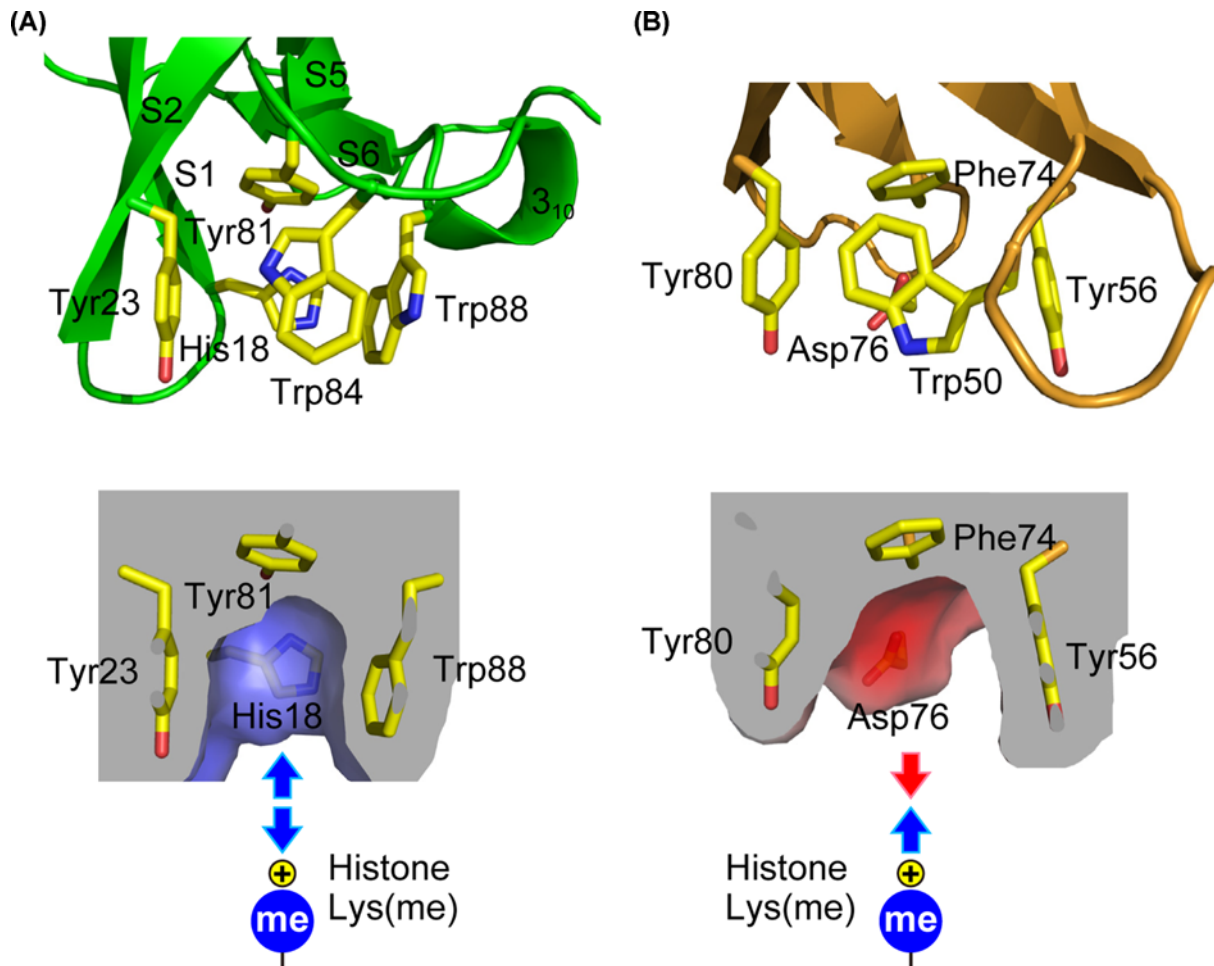


Figure 3. Structural comparison of aromatic binding sites for methyl-lysine of the histone tail

(A) The aromatic binding cage of Eaf3 CD. (B) The aromatic binding cage of the Phf19 Tudor domain [35]. Top: residues that form the binding cage. Bottom: sliced view of the molecular surface showing electrostatic potential (blue: positive, red: negative).

A unique histidine residue in the binding site

All methylated-lysine histone-binding modules have a characteristic binding cage consisting of two to four aromatic residues (Phe, Tyr and Trp), which contact a methylammonium moiety through cation- π and van der Waals interactions [34].

The structure of Eaf3 CD has been previously determined and the binding of Eaf3 to H3K36me found to be weak [14,33]. We re-examined both the dynamic and static structures of Eaf3 CD by using NMR spectroscopy (Supplementary Table S2 and Figure S1a). The present NMR structure was consistent with the previous solved structures, although it resembled the crystal structure more than the solution one (Supplementary Figure S2). Unlike HP1 and Polycomb CDs, where a methylated H3 tail is inserted in a cleft, the corresponding cleft in Eaf3 CD is occupied by β strand S1, and helix H2 is positioned above the S1 strand (Supplementary Figure S1c). In addition, relaxation analysis indicated that there is restricted backbone motion on the picosecond to nanosecond timescale for all regions except for the N- and C-termini (residues 1–8 and 115–120) and a long loop between β strands S3 and S4 (residues 43–57) (Supplementary Figure S1d). The two turns between β strands S1 and S2 and between S5 and S6, which form the binding pocket (Supplementary Figure S1a, marked by dashed line), show a relatively low degree of flexibility as normal (Supplementary Figure S1d, marked by dashed lines). It is therefore clear that the origin of the weak binding of Eaf3 CD is not related to the dynamic character of this domain.

Eaf3 CD possesses an aromatic cage formed by Tyr81 at the bottom with Tyr23, Trp84 and Trp88 around the walls (Figure 3A). A previous study of Eaf3 CD bound to a H3K36me₂ analog, in which Eaf3 CD was engineered to link to a H3K36 fragment to a chemically incorporated methyl-lysine analogue produced by cysteine alkylation, revealed

Table 2 Dissociation constant (K_d) for the binding of Eaf3 CD variants to methylated histone H3 peptide

Eaf3 CD	H3K36me3 K_d (μ M)	H3K4me3 K_d (μ M)	H3R2ame2K4me3 K_d (μ M)
Wild-type	1880 \pm 130	2900 \pm 10	1360 \pm 20
G19A	760 \pm 40	800 \pm 70	430 \pm 40
Y23A	N.B.	N.B.	N.B.
Y81A	N.B.	N.B.	N.B.
Q82A	1650 \pm 70	2240 \pm 280	1260 \pm 60
W84A	N.B.	N.B.	N.B.
W84Y	1200 \pm 60	1590 \pm 280	760 \pm 20
W88A	N.B.	N.B.	N.B.

N.B.: not bound.

that these four aromatic residues (Tyr23, Tyr81, Trp84 and Trp88) surround the dimethyl-lysine analog [14]. In fact, each of the four aromatic residues was found to be essential for the interaction because the alanine mutants Y23A, Y81A, W84A and W88A, each of which maintain the proper conformation (Supplementary Figure S3), failed to bind to a trimethylated (me3) H3K36, H3K4me3 or H3R2ame2K4me3 peptide (Table 2 and Supplementary Figure S4). By contrast, W84Y and two alanine mutants of Gly19 and Gln82, both of which are near to the aromatic cage but not involved in direct binding, maintained the binding ability of Eaf3 CD.

Taken together, the above results indicate that Eaf3 CD *per se* has few direct contacts with histone residues and relies heavily on the interaction with a methyl-lysine. We therefore focused on the residues inside the binding cage of Eaf3 CD. To identify unique features, we first compared the structures of histone methyl-lysine peptide complexes determined so far. Supplementary Table S3 summarizes the results of a systematic survey of residues in which the heavy atoms of the side-chains of the methyl-lysine-binding domains are within 6 Å of the N ζ atom of the methyl-lysine of histone. As expected, all histone-binding domains contain aromatic residues [34]. Curiously, however, Eaf3 CD possesses a histidine, His18, and not an acidic residue as the charged amino acid (Figure 3A and Supplementary Table S4). In general, a histidine residue will be protonated at physiological pH, which would produce a repulsive Coulombic barrier to interacting with the positively charged methyl-lysine of histone. Contrary to Eaf3 CD, acidic residues are often observed in the binding aromatic cages of other methyl-lysine-binding modules (Supplementary Table S3 and Figure 3B). Notably, the electrostatically unfavorable histidine residue in the binding cage is not limited to yeast Eaf3, and is seen in other species such as animals and plants (Supplementary Figure S5).

Physiological pK_a of His18 in the binding site of Eaf3 CD

The structural analysis suggested that the unusual His18 residue in the aromatic cage might be a key determinant for the weak interactions of Eaf3 CD. However, a histidine residue has a wide range of acid dissociation constant (pK_a) values depending on its environment. Next, therefore, we determined the pK_a value of His18 (Figure 4A–D) and its tautomeric state (Figure 4E) by using NMR [36]. We confirmed that no disruption of structure was caused by the pH changes throughout the experiments (not shown). The observed pK_a value of His18 was approximately 6.8 (Figure 4D), indicating that the binding activity of the aromatic cage of Eaf3 CD is sensitive to changes in pH under physiological conditions.

Protonation state of His18 facilitates pH-dependent binding of Eaf3 CD

To verify the pH-dependent binding of Eaf3 CD suggested by the above observations, we examined the interaction of Eaf3 CD with methylated histone peptide under different pH (Figure 5A). An increase in pH from 6.8 to 7.5 enhanced the binding of Eaf3 CD to H3K36me3 2.2-fold. Upon a further increase to pH 8.5, the binding was enhanced a further 3.6-fold. In contrast, a decrease from pH 6.8 to 6.0 weakened the binding 2.3-fold. Decreasing the pH to 5.2, where almost all Eaf3 CD molecules would contain protonated His18, abolished the binding. Thus, the protonation state of His18 is negatively correlated with the binding activity of Eaf3 CD. At a physiological pH of 6.8, almost half of all Eaf3 CD molecules will be protonated at His18 and thus in an inactive binding form, while the rest will be deprotonated at His18 and therefore in an active binding form.

We further confirmed the necessity of protonation of His18 in the observed pH sensitivity of binding by examining the binding activity of H18A and H18D at pH 6.8, 8.5 and 5.2 (Figure 5B,C). In contrast with the alanine mutants of the four cage aromatic residues, none of which showed binding (Table 2), H18A showed 2.9-fold stronger binding to

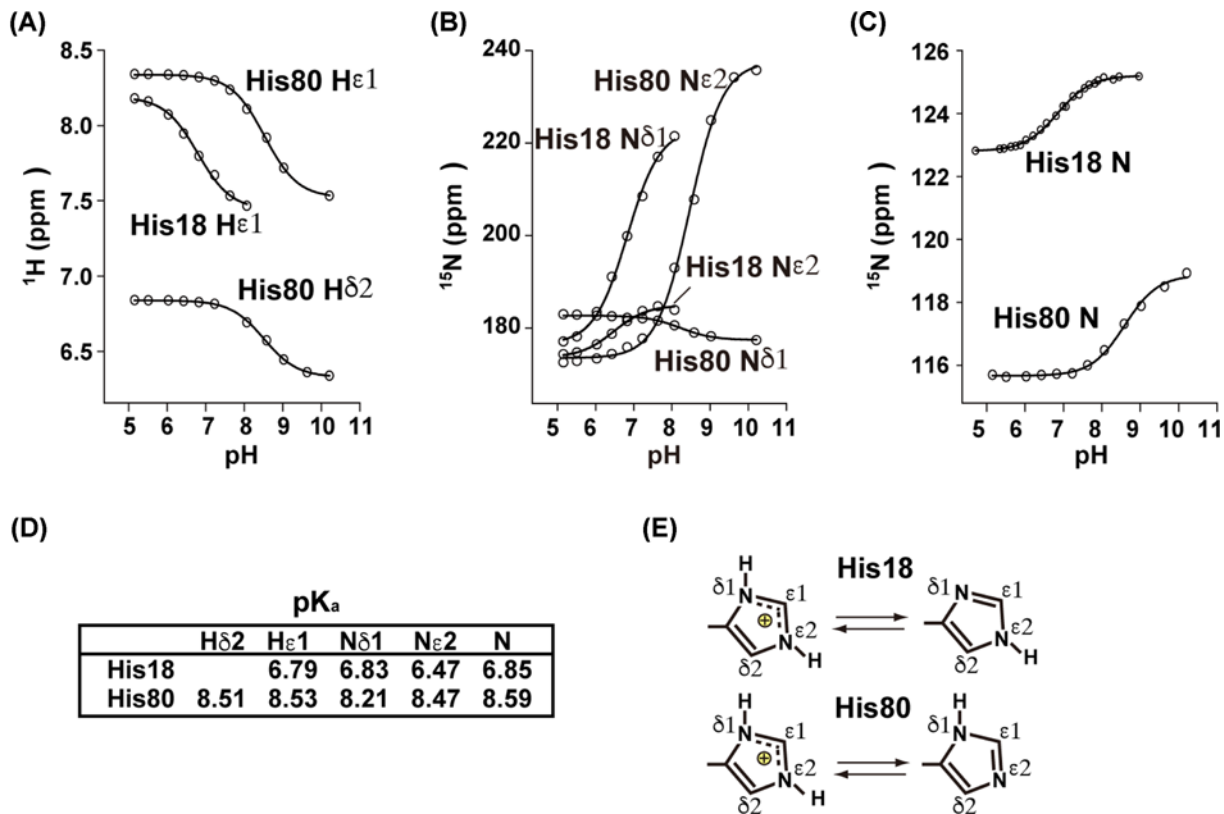


Figure 4. pK_a values and tautomeric states of the histidine residues of Eaf3 CD

Shown are the pH titration curves for ¹H and ¹⁵N atoms of the two histidine residues of Eaf3 CD. (A) Side chain Hδ2 and Hε1. (B) Side-chain Nδ1 and Nε2. (C) Main-chain N. (D) Calculated pK_a values. (E) Determined tautomeric states of the two histidine residues.

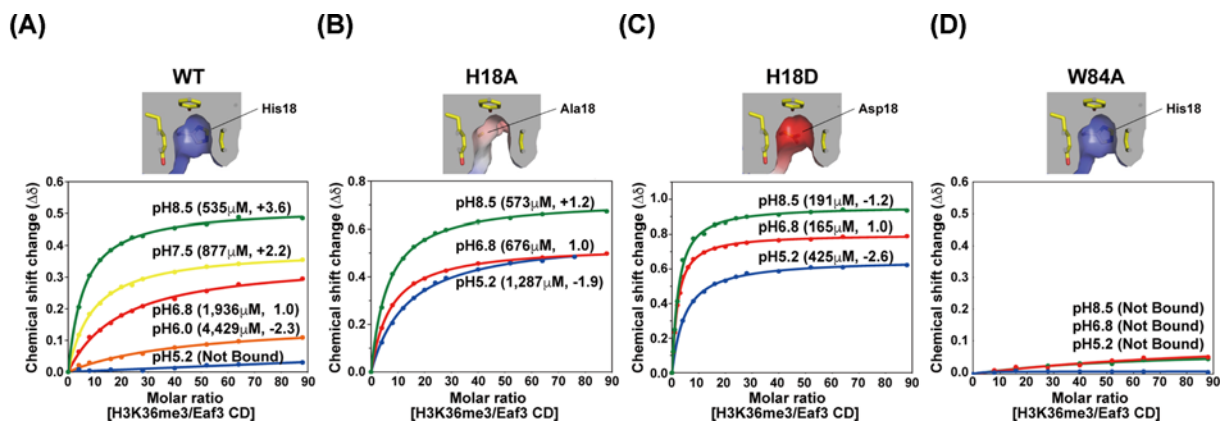


Figure 5. NMR titration of Eaf3 CD with H3K36me3 peptide at different pH

(A) WT Eaf3 CD, (B) H18A Eaf3 CD, (C) H18D Eaf3 CD and (D) W84A Eaf3 CD. Titration curves are plotted for Ala25 of Eaf3 CD. The calculated K_d and fold changes for binding at pH 6.8 are given in parentheses.

the H3K36me3 peptide as compared with the WT peptide at pH 6.8 (Figure 5A,B). Relative to pH 6.8, the binding of H18A to H3K36me3 peptide was slightly enhanced by a factor of 1.2-fold at pH 8.5, and decreased by 1.9-fold at pH 5.2 (Figure 5B), although pH 5.2 did not result in a complete loss of activity of Eaf3 CD, unlike WT (Figure 5A). H18D enhanced the binding to H3K36me3 peptide even more (Figure 5C,B), with an 11.7-fold increase relative to WT at pH 6.8 (Figure 5A,C). H18D maintained high-binding activity at pH 8.5 and to a lesser extent at pH 5.2

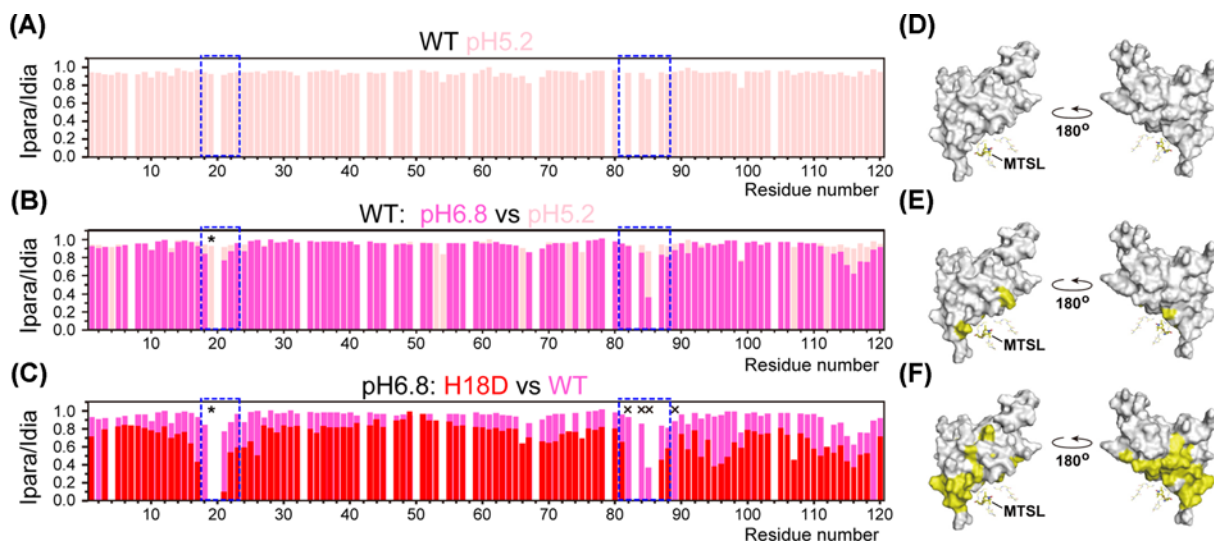


Figure 6. Paramagnetic relaxation enhancement profiles of Eaf3 CD mixed with MTSL spin-labeled H3K36me3 peptide
(A–C) Intensity ratio (I_{para}/I_{dia}) of ^{15}N -labeled Eaf3 CD residues when mixed with H3K36me3 peptide labeled with either paramagnetic (para) or diamagnetic (dia) MTSL. The intensity ratio is normalized with the maximum at 1.0. Blue dotted line indicates the position of the aromatic binding cage. (A) WT Eaf3 CD, measured at pH 5.2 (pink). (B) Comparison between WT Eaf3 CD at pH 6.8 (magenta) and WT Eaf3 CD at pH 5.2 (pink). (C) Comparison between H18D Eaf3 CD at pH 6.8 (red) and WT Eaf3 CD at pH 6.8 (magenta). Asterisks indicate residues absent in the paramagnetic state. 'X' indicates a residue absent in both paramagnetic and diamagnetic states. Blank spaces are either proline residues or residues for which peak intensity was not measured because the signals overlapped or were unassigned. (D–F) Residues exhibiting $I_{para}/I_{dia} < 0.7$ (yellow) mapped on the structure. (D) WT Eaf3 CD, measured at pH 5.2. (E) WT Eaf3 CD, measured at pH 6.8. (F) H18D Eaf3 CD, measured at pH 6.8. The position of MTSL is determined by back calculation using the PRE data of H18D [37].

(Figure 5C). In addition, the electrostatic state in the aromatic binding cage of the mutant proteins altered the preference for H3K36me3 (Supplementary Figure S6). As described above (Table 1), WT Eaf3 CD showed a preference for H3K36me3 over H3K36me2 (Supplementary Figure S6a). H18A exhibited the same preference (Supplementary Figure S6b), whereas H18D showed a preference for the dimethyl form over the trimethyl one (Supplementary Figure S6c). For binding to H3K36me2 peptide, H18D exhibited a 71.1-fold stronger binding as compared with WT (Supplementary Figure S6c and a). Thus, the introduction of negative charge into the binding cage of Eaf3 CD greatly augmented the binding activity, disrupted the pH sensitivity and altered the preference to H3K36me3.

We also tested the pH dependence of W84A as a representative of alanine mutants of the four binding aromatic residues in the binding site. Similar to the observations at pH 6.8 (Table 2), W84A showed no binding at pH 8.5 or at pH 5.2, demonstrating the pH independence of mutant W84A regardless of His18 de-protonation (Figure 5D).

Dual function of Eaf3 CD as a pH_i sensor and a histone-binding module

The above findings showed that His18 is the crucial structure determinant of the weak binding of Eaf3 CD. At the same time, they demonstrated a novel function of Eaf3 CD as a pH_i sensor with histone methyl-lysine-binding ability. We therefore investigated this dual function from the viewpoint of the structure by using paramagnetic relaxation enhancement (PRE) experiments. In PRE, effects are observed depending only on the distance between the paramagnetic center and the proton; thus, it is possible to obtain structural information about low-population states in an exchanging system such as that of Eaf3 CD and H3K36me3 peptide [37].

The addition of an H3K36me3 peptide carrying an MTSL spin label to 0.3 mM ^{15}N -labeled Eaf3 CD at a molar ratio of 1:1 gave rise to only subtle chemical shift changes of the backbone amide signals for a few residues of Eaf3 CD (Figure 6). At pH 5.2, no PRE effects were observed, indicating no binding (Figure 6A,D). At pH 6.8, by contrast, signals from several specific residues around the binding site were broadened upon addition of the paramagnetically labeled H3K36me3 peptide (Figure 6B,E). For the H18D mutation at pH 6.8, many broadened signals were also observed in the binding site and surrounding area (Figure 6C,F). Taking all the findings together, we conclude that Eaf3 CD is a previously unknown pH_i sensor that detects a change in pH_i and simultaneously converts it into methylated histone-binding ability via protonation of His18 in the binding site.

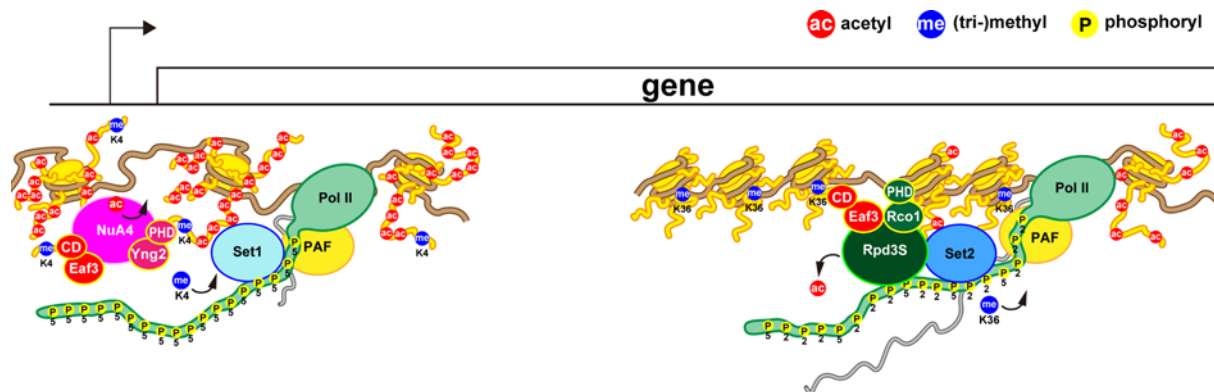


Figure 7. Schematic view of the regulation of gene expression in yeast cells

At promoter regions, Set1 methyltransferase (COMPASS complex), which is associated with the Ser5-phosphorylated C-terminal domain (CTD) of the largest subunit of the Pol II and PAF transcription elongation complex, methylates H3K4 of a nucleosome; NuA4 histone acetyltransferase is then recruited to the H3K4me-nucleosome and activated by the cooperative binding of Eaf3 CD, Yng2 PHD, and probably specific domains of the other subunits of NuA4; finally, NuA4 acetylates the nucleosome for efficient transcription initiation. In coding regions, Set2 methyltransferase, which is associated with the Ser2,Ser5-phosphorylated CTD of Pol II, methylates H3K36 of a nucleosome; Rpd3S histone deacetylase is then recruited to the H3K36me-nucleosome through its association with the Set2 and Ser2,Ser5-phosphorylated CTD of Pol II, and activated by cooperative binding of Eaf3 CD and Rco1 PHD; finally, Rpd3S deacetylates the nucleosome to repress spurious transcription from cryptic start sites. To reduce complexity, many of the other chromatin and transcription factors are not depicted.

Discussion

Eaf3 CD offers pH sensitivity to the regulation of HAT/HDAC activity

As described above and in previous studies [9,10,14,33], Eaf3 CD itself has high methylation specificity but low sequence specificity; therefore, combinatorial actions with the PHD of Yng2 in NuA4 and with the PHD of Rco1 in Rpd3S are necessary for the overall affinity and specificity of the H3K4me- and H3K36me-nucleosome interaction [12,16], and activation [15,38,39] of the complexes (Figure 7). A biochemical study previously demonstrated that Rpd3S preferentially binds di-nucleosomes by contacting two nucleosomes simultaneously via Eaf3 CD and Rco1 PHD [40]. Deuterium exchange mass spectrometry study also found that Rpd3S undergoes conformational changes upon contact with nucleosomes, and the Sin3-interacting domain of Rco1 allosterically stimulates preferential binding of Eaf3 CD to H3K36me [13]. These findings strongly suggest that the precise positioning of the complex on nucleosomes by multiple domains is crucial for regulation of the enzymatic activity. Our findings now open up the possibility that Eaf3 CD provides pH sensitivity to this regulation. We suspect that Eaf3 CD is needed to swiftly respond to cellular signals of pH_i perturbation and coordinate co-transcriptional chromatin remodeling. For instance, during cell proliferation when the pH_i increases, subsets of genes should be activated, requiring both dynamic opening of promoter regions by HAT for easy access of Pol II, and tight closing of coding regions by HDAC after Pol II passes through to avoid aberrant gene transcripts. Via His18, Eaf3 CD senses increasing pH_i and simultaneously strengthens its affinity for methylated nucleosomes, thereby placing NuA4 and Rpd3S in the appropriate position on the nucleosomes in combination with other subunits. Activated NuA4 on promoter regions and Rpd3S on coding regions establish an environment for efficient transcription. The generation of acetate during the histone deacetylation process might promote dissociation of Rpd3S from nucleosomes in the gene bodies. Further studies are needed to verify this notion.

Generality of the function of the pH_i sensor activity of Eaf3 CD beyond yeast cells

In addition to Eaf3, *S. cerevisiae* has two well-known CD-containing proteins: Chd1, an ATP-dependent chromatin remodeling factor; and Esa1, the catalytic subunit of HAT NuA4. In previous studies, we found that both CDs are structurally incompetent to bind to lysine-methylated histone [41,42]. Given the fact that Eaf3 is a limited CD protein possessing methylated histone-binding ability in yeast, its pH-responsive interactions may have a fundamental role. This idea is supported by the fact that the significance of fluctuations in pH_i is not limited to yeast. In higher

eukaryotes, changes in pH_i have been correlated with cell proliferation [43], differentiation [44], cell cycle progression [45], apoptosis [7] and cancer [46]. In this regard, it is worth noting that His18 of Eaf3 CD is highly conserved (Supplementary Figure S5) and the corresponding histidine of Eaf3 orthologs – namely, His21 in human MRG15, His62 in *Arabidopsis* MRG2, and His37 in rice MRG701 – actually lies at a structurally equivalent position [47–49]. In addition, the interactions between MRG15 CD and methyl-lysine peptides have been found to be strongly sensitive to the pH used for NMR titrations, with little or no interaction between MRG15 CD and H3K36me3 peptide at acidic pH [50]. On the basis of these observations, we predict that all MRG protein CDs essentially functions as a pH_i sensor identical with the role of Eaf3 CD described here.

Finally, to explore pH_i sensor activity and the correlation between pH_i and histone acetylation, we focused here on the histone methyl-lysine-binding domain and one of its histidine residues. However, this does not mean that Eaf3 CD is the only domain that acts as a pH_i sensor. It is noteworthy that the PHDs of human Death Inducer Obliterator 3 (Dido3) and its *Drosophila* ortholog PPS use a histidine to bind trimethylated H3K4 and exhibit pH dependence [51,52]. The *Arabidopsis* SHH1 tandem Tudor domain also contains a histidine in its aromatic binding cage for methylated H3K9 [53]. We speculate that other chromatin-associated proteins might use a similar pH-responsive mechanism to regulate chromatin structure.

Competing Interests

The authors declare that there are no competing interests associated with the manuscript.

Funding

This work was supported in part by Grants-in-Aid for an NMR platform [grant number 07022019 (to Y.N.)] from the Ministry of Education, Culture, Sports, Science and Technology (MEXT), Japan; Basis for Supporting Innovative Drug Discovery and Life Science Research (BINDS) from the Japan Agency for Medical Research and Development (AMED), Japan under [grant number JP17am0101073 (to Y.N.)].

Author Contribution

M.O. conceptualized the study, performed the experiments, analyzed the data, and wrote the manuscript. Y.N. formulated the project, supervised the research, and reviewed the manuscript.

Database Depositions

Coordinates for the solution structures of Eaf3 CD have been deposited in the RCSB Protein Data Bank with accession number 6K5W. NMR factors have been deposited in the Biological Magnetic Resonance Bank with accession number 36261.

Abbreviations

ac, acetylated; ame2, arginine-asymmetrically dimethylated; CD, chromodomain; Eaf3, essential Sas2-related acetyltransferase1-associated factor 3; H3, histone H3; H4, histone H4; HAT, histone acetyl transferase; HDAC, histone deacetylase; HSQC, heteronuclear single quantum coherence; K_d , dissociation constant; me2, dimethylated; me3, trimethylated; NMR, nuclear magnetic resonance; NOE, nuclear overhauser effect; pH_i , intracellular pH; pho, phosphorylated; Pol II, RNA polymerase II; pK_a , acid dissociation constant; PRE, paramagnetic relaxation enhancement; WT, wild-type.

References

- Kouzarides, T. (2007) Chromatin modifications and their function. *Cell* **128**, 693–705, <https://doi.org/10.1016/j.cell.2007.02.005>
- Strahl, B.D. and Allis, C.D. (2000) The language of covalent histone modifications. *Nature* **403**, 41–45, <https://doi.org/10.1038/47412>
- Pokholok, D.K., Harbison, C.T., Levine, S., Cole, M., Hannett, N.M., Lee, T.I. et al. (2005) Genome-wide map of nucleosome acetylation and methylation in yeast. *Cell* **122**, 517–527, <https://doi.org/10.1016/j.cell.2005.06.026>
- Roby, D., Suka, Y., Xenarios, I., Kurdistani, S.K., Wang, A., Suka, N. et al. (2002) Microarray deacetylation maps determine genome-wide functions for yeast histone deacetylases. *Cell* **109**, 437–446, [https://doi.org/10.1016/S0092-8674\(02\)00746-8](https://doi.org/10.1016/S0092-8674(02)00746-8)
- Hampsey, M. and Reinberg, D. (2003) Tails of intrigue: phosphorylation of RNA polymerase II mediates histone methylation. *Cell* **113**, 429–432, [https://doi.org/10.1016/S0092-8674\(03\)00360-X](https://doi.org/10.1016/S0092-8674(03)00360-X)
- McBrien, M.A., Behbahan, I.S., Ferrari, R., Su, T., Huang, T.W., Li, K. et al. (2013) Histone acetylation regulates intracellular pH. *Mol. Cell* **49**, 310–321, <https://doi.org/10.1016/j.molcel.2012.10.025>
- Lagadic-Gossman, D., Huc, L. and Lecœur, V. (2004) Alterations of intracellular pH homeostasis in apoptosis: origins and roles. *Cell Death Differ.* **11**, 953–961, <https://doi.org/10.1038/sj.cdd.4401466>
- Grinstein, S., Rotin, D. and Mason, M.J. (1989) Na^+/H^+ exchange and growth factor-induced cytosolic pH changes. Role in cellular proliferation. *Biochim. Biophys. Acta* **988**, 73–97, [https://doi.org/10.1016/0304-4157\(89\)90004-X](https://doi.org/10.1016/0304-4157(89)90004-X)

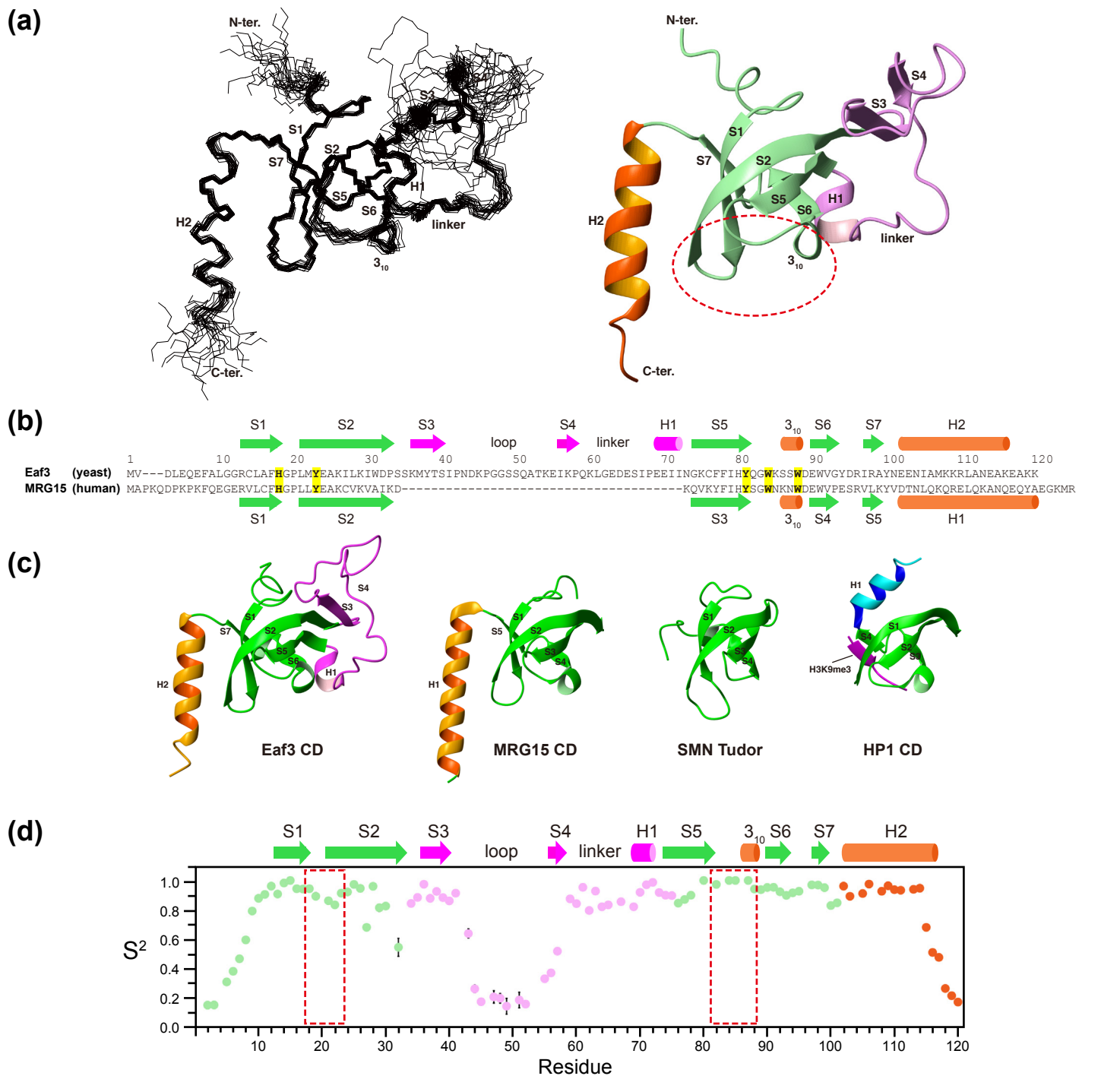
- 9 Carrozza, M.J., Li, B., Florens, L., Suganuma, T., Swanson, S.K., Lee, K.K. et al. (2005) Histone H3 methylation by Set2 directs deacetylation of coding regions by Rpd3S to suppress spurious intragenic transcription. *Cell* **123**, 581–592, <https://doi.org/10.1016/j.cell.2005.10.023>
- 10 Joshi, A.A. and Struhl, K. (2005) Eaf3 chromodomain interaction with methylated H3-K36 links histone deacetylation to Pol II elongation. *Mol. Cell* **20**, 971–978, <https://doi.org/10.1016/j.molcel.2005.11.021>
- 11 Keogh, M.C., Kurdستاني, S.K., Morris, S.A., Ahn, S.H., Podolny, V., Collins, S.R. et al. (2005) Cotranscriptional set2 methylation of histone H3 lysine 36 recruits a repressive Rpd3 complex. *Cell* **123**, 593–605, <https://doi.org/10.1016/j.cell.2005.10.025>
- 12 Li, B., Gogol, M., Carey, M., Lee, D., Seidel, C. and Workman, J.L. (2007) Combined action of PHD and chromo domains directs the Rpd3S HDAC to transcribed chromatin. *Science* **316**, 1050–1054, <https://doi.org/10.1126/science.1139004>
- 13 Ruan, C., Lee, C.H., Cui, H., Li, S. and Li, B. (2015) Nucleosome contact triggers conformational changes of Rpd3S driving high-affinity H3K36me nucleosome engagement. *Cell Rep.* **10**, 204–215, <https://doi.org/10.1016/j.celrep.2014.12.027>
- 14 Xu, C., Cui, G., Botuyan, M.V. and Mer, G. (2008) Structural basis for the recognition of methylated histone H3K36 by the Eaf3 subunit of histone deacetylase complex Rpd3S. *Structure* **16**, 1740–1750, <https://doi.org/10.1016/j.str.2008.08.008>
- 15 Steunou, A.L., Cramet, M., Rossetto, D., Aristizabal, M.J., Lacoste, N., Drouin, S. et al. (2016) Combined action of histone reader modules regulates NuA4 local acetyltransferase function but not its recruitment on the genome. *Mol. Cell. Biol.* **36**, 2768–2781, <https://doi.org/10.1128/MCB.00112-16>
- 16 Su, W.P., Hsu, S.H., Chia, L.C., Lin, J.Y., Chang, S.B., Jiang, Z.D. et al. (2016) Combined Interactions of plant homeodomain and chromodomain regulate NuA4 activity at DNA double-strand breaks. *Genetics* **202**, 77–92, <https://doi.org/10.1534/genetics.115.184432>
- 17 Reid, J.L., Moqtaderi, Z. and Struhl, K. (2004) Eaf3 regulates the global pattern of histone acetylation in *Saccharomyces cerevisiae*. *Mol. Cell. Biol.* **24**, 757–764, <https://doi.org/10.1128/MCB.24.2.757-764.2004>
- 18 Cavanagh, J., Fairbrother, W.J., Palmer, III, A.G. and Skelton, N.J. (2006) *Protein NMR Spectroscopy: Principles and Practice*, 2nd edn, Academic Press, San Diego, CA
- 19 Yamazaki, T., Forman-Kay, J.D. and Kay, L.E. (1993) Two-dimensional NMR experiments for correlating $^{13}\text{C}\beta$ and $^1\text{H}\delta/\epsilon$ chemical shifts of aromatic residues in ^{13}C -labeled proteins via scalar coupling. *J. Am. Chem. Soc.* **115**, 11054–11055, <https://doi.org/10.1021/ja00076a099>
- 20 Prompers, J.J., Groenewegen, A., Hilbers, C.W. and Pepermans, H.A.M. (1998) Two-dimensional NMR experiments for the assignment of aromatic side chains in ^{13}C -labeled proteins. *J. Magn. Reson.* **130**, 68–75, <https://doi.org/10.1006/jmre.1997.1277>
- 21 Krichna, N.R. and Berliner, L.J. (1998) *Biological Magnetic Resonance 16*, Kluwer Academic/Plenum Publishers, New York
- 22 Delaglio, F., Grzesiek, S., Vuister, G.W., Zhu, G., Pfeifer, J. and Bax, A. (1995) NMRPipe: A multidimensional spectral processing system based on UNIX pipes. *J. Biomol. NMR* **6**, 277–293
- 23 Johnson, B.A. and Blevins, R.A. (1994) NMRView: a computer program for the visualization and analysis of NMR data. *J. Biomol. NMR* **4**, 603–614, <https://doi.org/10.1007/BF00404272>
- 24 Cornilescu, G., Delaglio, F. and Bax, A. (1999) Protein backbone angle restraints from searching a database for chemical shift and sequence homology. *J. Biomol. NMR* **13**, 289–302, <https://doi.org/10.1023/A:1008392405740>
- 25 Brünger, A.T. (1993) *X-PLOR Version 3.1: A System for X-Ray Crystallography and NMR*, Yale University Press, New Haven, CT
- 26 Schwieters, C.D., Kuszewski, J.J., Tjandra, N. and Clore, G.M. (2003) The Xplor-NIH NMR molecular structure determination package. *J. Magn. Reson.* **160**, 65–73, [https://doi.org/10.1016/S1090-7807\(02\)00014-9](https://doi.org/10.1016/S1090-7807(02)00014-9)
- 27 Linge, J.P., Williams, M.A., Spronk, C.A., Bonvin, A.M. and Nilges, M. (2003) Refinement of protein structures in explicit solvent. *Proteins* **50**, 496–506, <https://doi.org/10.1002/prot.10299>
- 28 Laskowski, R.A., Rullmann, J.A.C., MacArthur, M.W., Kaptein, R. and Thornton, J.M. (1996) AQUA and PROCHECK-NMR: Programs for checking the quality of protein structures solved by NMR. *J. Biomol. NMR* **8**, 477–486
- 29 Koradi, R., Billeter, M. and Wüthrich, K. (1996) MOLMOL: A program for display and analysis of macromolecular structures. *J. Mol. Graph.* **14**, 51–55, [https://doi.org/10.1016/0263-7855\(96\)00009-4](https://doi.org/10.1016/0263-7855(96)00009-4)
- 30 Mandel, A.M., Akke, M. and Palmer, III, A.G. (1995) Backbone dynamics of *Escherichia coli* ribonuclease HI: correlations with structure and function in an active enzyme. *J. Mol. Biol.* **246**, 144–163, <https://doi.org/10.1006/jmbi.1994.0073>
- 31 Tjandra, N., Feller, S.E., Pastor, R.W. and Bax, A. (1995) Rotational diffusion anisotropy of human ubiquitin from ^{15}N NMR relaxation. *J. Am. Chem. Soc.* **117**, 12562–12566, <https://doi.org/10.1021/ja00155a020>
- 32 Cole, R. and Loria, J.P. (2003) FAST-Modelfree: a program for rapid automated analysis of solution NMR spin relaxation data. *J. Biomol. NMR* **26**, 203–213, <https://doi.org/10.1023/A:1023808801134>
- 33 Sun, B., Hong, J., Zhang, P., Dong, X., Shen, X., Lin, D. et al. (2008) Molecular basis of the interaction of *Saccharomyces cerevisiae* Eaf3 chromo domain with methylated H3K36. *J. Biol. Chem.* **283**, 36504–36512, <https://doi.org/10.1074/jbc.M806564200>
- 34 Taverna, S.D., Li, H., Ruthenburg, A.J., Allis, C.D. and Patel, D.J. (2007) How chromatin-binding modules interpret histone modifications: lessons from professional pocket pickers. *Nat. Struct. Mol. Biol.* **14**, 1025–1040, <https://doi.org/10.1038/nsmb.1338>
- 35 Ballaré, C., Lange, M., Lapinaite, A., Martin, G.M., Morey, L., Pascual, G. et al. (2012) Phf19 links methylated Lys36 of histone H3 to regulation of Polycomb activity. *Nat. Struct. Mol. Biol.* **19**, 1257–1265, <https://doi.org/10.1038/nsmb.2434>
- 36 Pelton, J.G., Torchia, D.A., Meadow, N.D. and Roseman, S. (1993) Tautomeric states of the active-site histidines of phosphorylated and unphosphorylated IIIgIc, a signal-transducing protein from *Escherichia coli*, using two-dimensional heteronuclear NMR techniques. *Protein Sci.* **2**, 543–558
- 37 Iwahara, J. and Clore, G.M. (2006) Detecting transient intermediates in macromolecular binding by paramagnetic NMR. *Nature* **440**, 1227–1230, <https://doi.org/10.1038/nature04673>
- 38 Drouin, S., Laramée, L., Jacques, P.E., Forest, A., Bergeron, M. and Robert, F. (2010) DSIF and RNA polymerase II CTD phosphorylation coordinate the recruitment of Rpd3S to actively transcribed genes. *PLoS Genet.* **6**, e1001173, <https://doi.org/10.1371/journal.pgen.1001173>

- 39 Govind, C.K., Qiu, H., Ginsburg, D.S., Ruan, C., Hofmeyer, K., Hu, C. et al. (2010) Phosphorylated Pol II CTD recruits multiple HDACs, including Rpd3C(S), for methylation-dependent deacetylation of ORF nucleosomes. *Mol. Cell* **39**, 234–246, <https://doi.org/10.1016/j.molcel.2010.07.003>
- 40 Huh, J.W., Wu, J., Lee, C.H., Yun, M., Gilada, D., Brautigam, C.A. et al. (2012) Multivalent di-nucleosome recognition enables the Rpd3S histone deacetylase complex to tolerate decreased H3K36 methylation levels. *EMBO J.* **31**, 3564–3574, <https://doi.org/10.1038/emboj.2012.221>
- 41 Okuda, M., Horikoshi, M. and Nishimura, Y. (2007) Structural polymorphism of chromodomains in Chd1. *J. Mol. Biol.* **365**, 1047–1062, <https://doi.org/10.1016/j.jmb.2006.10.039>
- 42 Shimojo, H., Sano, N., Moriwaki, Y., Okuda, M., Horikoshi, M. and Nishimura, Y. (2008) Novel structural and functional mode of a knot essential for RNA binding activity of the Esa1 presumed chromodomain. *J. Mol. Biol.* **378**, 987–1001, <https://doi.org/10.1016/j.jmb.2008.03.021>
- 43 Denker, S.P., Huang, D.C., Orłowski, J., Furthmayr, H. and Barber, D.L. (2000) Direct binding of the Na-H exchanger NHE1 to ERM proteins regulates the cortical cytoskeleton and cell shape independently of H+ translocation. *Mol. Cell* **6**, 1425–1436, [https://doi.org/10.1016/S1097-2765\(00\)00139-8](https://doi.org/10.1016/S1097-2765(00)00139-8)
- 44 Boussouf, A. and Gaillard, S. (2000) Intracellular pH changes during oligodendrocyte differentiation in primary culture. *J. Neurosci. Res.* **59**, 731–739, [https://doi.org/10.1002/\(SICI\)1097-4547\(20000315\)59:6%3c731::AID-JNR5%3e3.0.CO;2-G](https://doi.org/10.1002/(SICI)1097-4547(20000315)59:6%3c731::AID-JNR5%3e3.0.CO;2-G)
- 45 Putney, L.K. and Barber, D.L. (2003) Na-H exchange-dependent increase in intracellular pH times G2/M entry and transition. *J. Biol. Chem.* **278**, 44645–44649, <https://doi.org/10.1074/jbc.M308099200>
- 46 Stock, C. and Schwab, A. (2009) Protons make tumor cells like clockwork. *Pflugers Arch.* **458**, 981–992, <https://doi.org/10.1007/s00424-009-0677-8>
- 47 Zhang, P., Du, J., Sun, B., Dong, X., Xu, G., Zhou, J. et al. (2006) Structure of human MRG15 chromo domain and its binding to Lys36-methylated histone H3. *Nucleic Acids Res.* **34**, 6621–6628, <https://doi.org/10.1093/nar/gkl989>
- 48 Bu, Z., Yu, Y., Li, Z., Liu, Y., Jiang, W., Huang, Y. et al. (2014) Regulation of *Arabidopsis* flowering by the histone mark readers MRG1/2 via interaction with CONSTANS to modulate FT expression. *PLoS Genet.* **10**, e1004617, <https://doi.org/10.1371/journal.pgen.1004617>
- 49 Liu, Y., Wu, H., Yu, Y. and Huang, Y. (2016) Structural studies on MRG701 chromodomain reveal a novel dimerization interface of MRG proteins in green plants. *Protein Cell* **7**, 792–803, <https://doi.org/10.1007/s13238-016-0310-5>
- 50 Kumar, G.S., Chang, W., Xie, T., Patel, A., Zhang, Y., Wang, G.G. et al. (2012) Sequence requirements for combinatorial recognition of histone H3 by the MRG15 and Pf1 subunits of the Rpd3S/Sin3S corepressor complex. *J. Mol. Biol.* **422**, 519–531, <https://doi.org/10.1016/j.jmb.2012.06.013>
- 51 Gatchalian, J., Fütterer, A., Rothbart, S.B., Tong, Q., Rincon-Arango, H., Sánchez de Diego, A. et al. (2013) Dido3 PHD modulates cell differentiation and division. *Cell Rep.* **4**, 148–158, <https://doi.org/10.1016/j.celrep.2013.06.014>
- 52 Tencer, A.H., Gatchalian, J., Klein, B.J., Khan, A., Zhang, Y., Strahl, B.D. et al. (2017) A unique pH-dependent recognition of methylated histone H3K4 by PPS and DIDO. *Structure* **25**, 1530–1539, <https://doi.org/10.1016/j.str.2017.08.009>
- 53 Law, J.A., Du, J., Hale, C.J., Feng, S., Krajewski, K., Palanca, A.M. et al. (2013) Polymerase IV occupancy at RNA-directed DNA methylation sites requires SHH1. *Nature* **498**, 385–389, <https://doi.org/10.1038/nature12178>

Supplementary Figures and Tables

**The Eaf3 Chromodomain Acts as a pH Sensor for Gene Expression by
Altering its Binding Affinity for Histone Methylated-Lysine Residues**

Masahiko Okuda and Yoshifumi Nishimura



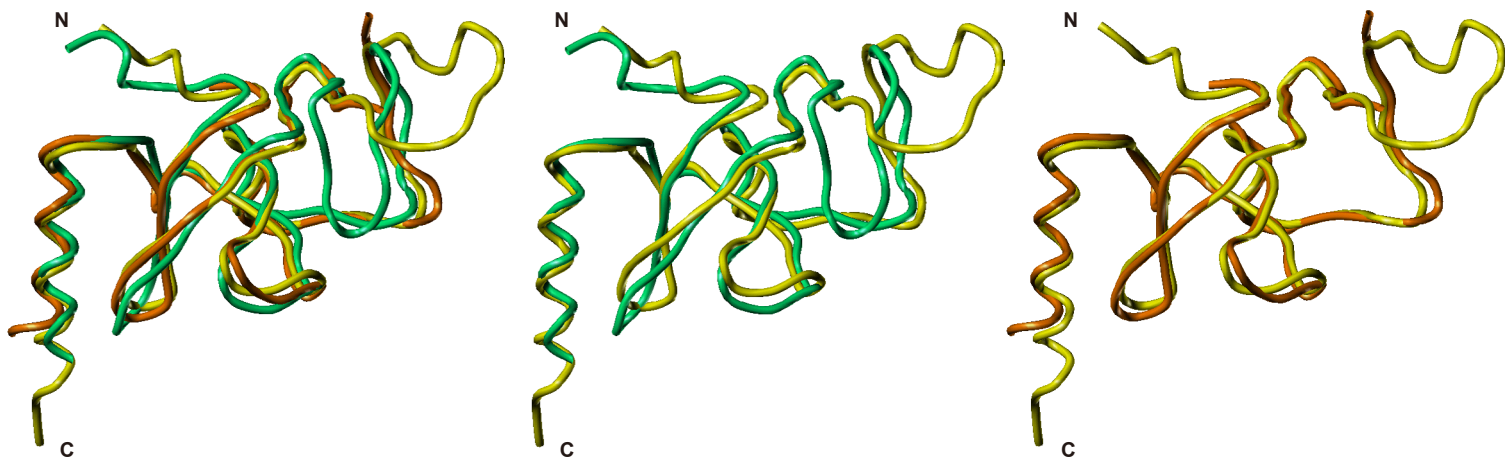
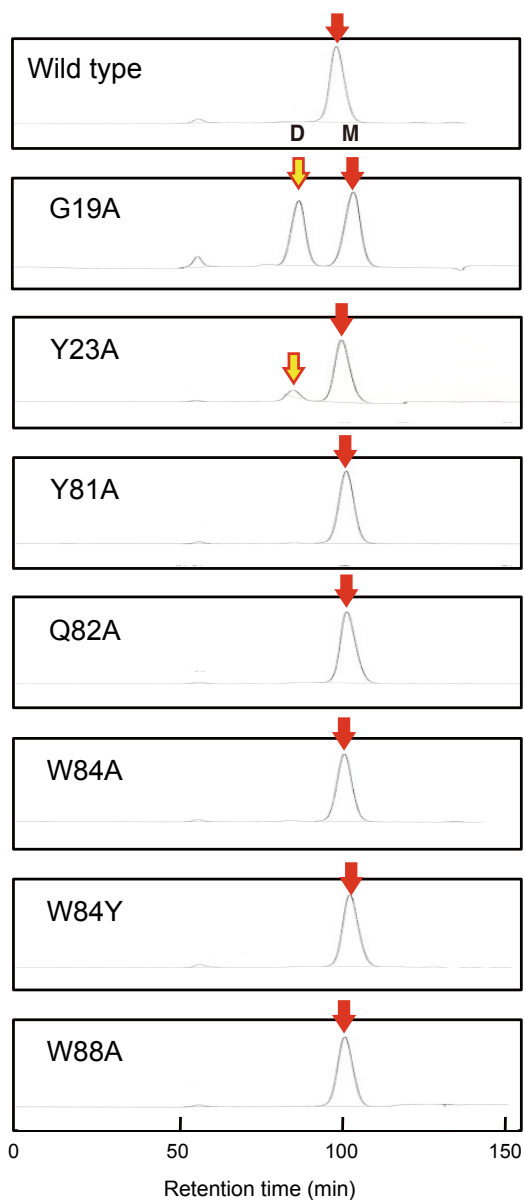
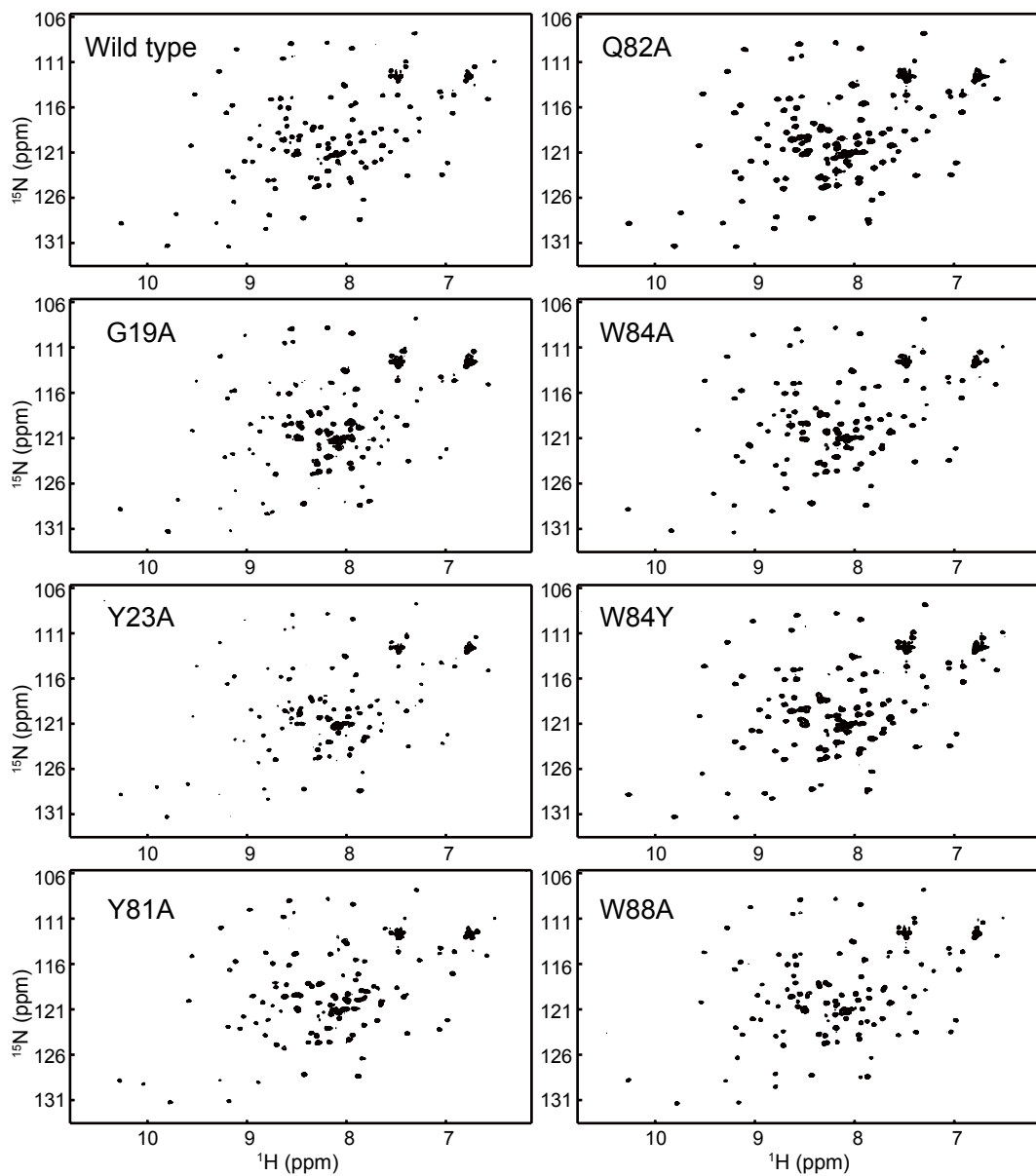


Fig. S2. Structure comparison of Eaf3 CDs.

Structural superposition of Eaf3 CDs. Yellow; this study, PDB ID: 6K5W. Green; PDB ID: 2K3X. Orange; PDB ID: 3K9F. Left; 6K5W v.s. 2K3X v.s. 3K9F. Middle; 6K5W v.s. 2K3X. Right; 6K5W v.s. 3K9F. Structures are superimposed for residues 11–42 and 56–113. R.s.m. deviations for the backbone structure between 6K5W and 2K3X, and between 6K5W and 3K9F were 1.62 Å and 1.07 Å, respectively.

(a)**(b)****Fig. S3. Preparation of site-directed mutants of Eaf3 CD.**

(a) Size exclusion chromatograms of wild-type and mutant Eaf3 CD. D: dimer, M: monomer.

(b) NMR ^1H , ^{15}N HSQC spectra of wild-type and mutant Eaf3 CD.

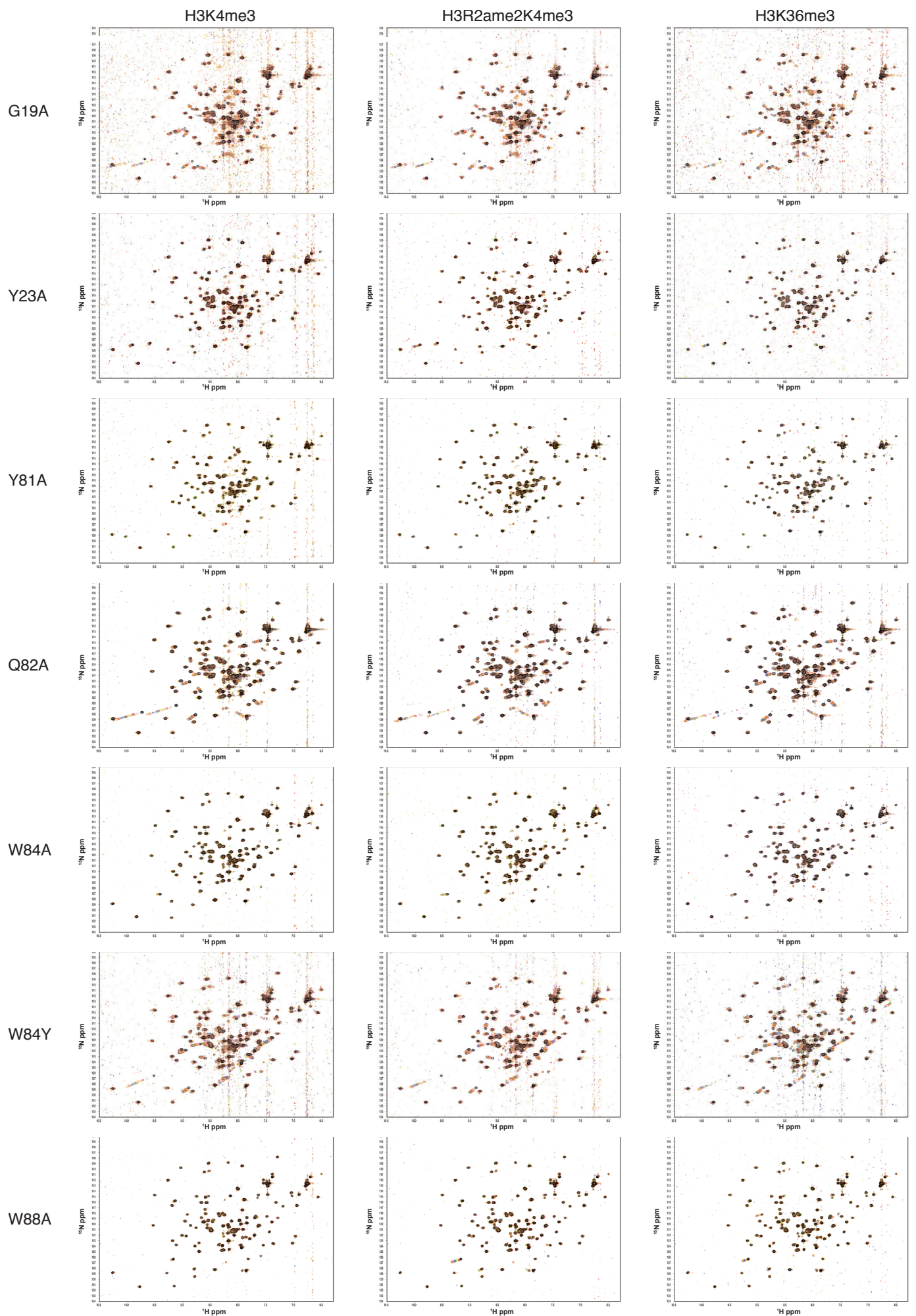


Fig. S4. NMR titration experiments.

Overlays of the ^1H , ^{15}N -HSQC spectra of Eaf3 CD mutants titrated with methylated H3 peptide. The methylated H3 peptides were added to each Eaf3 CD mutant at up to 88-fold molar excess.

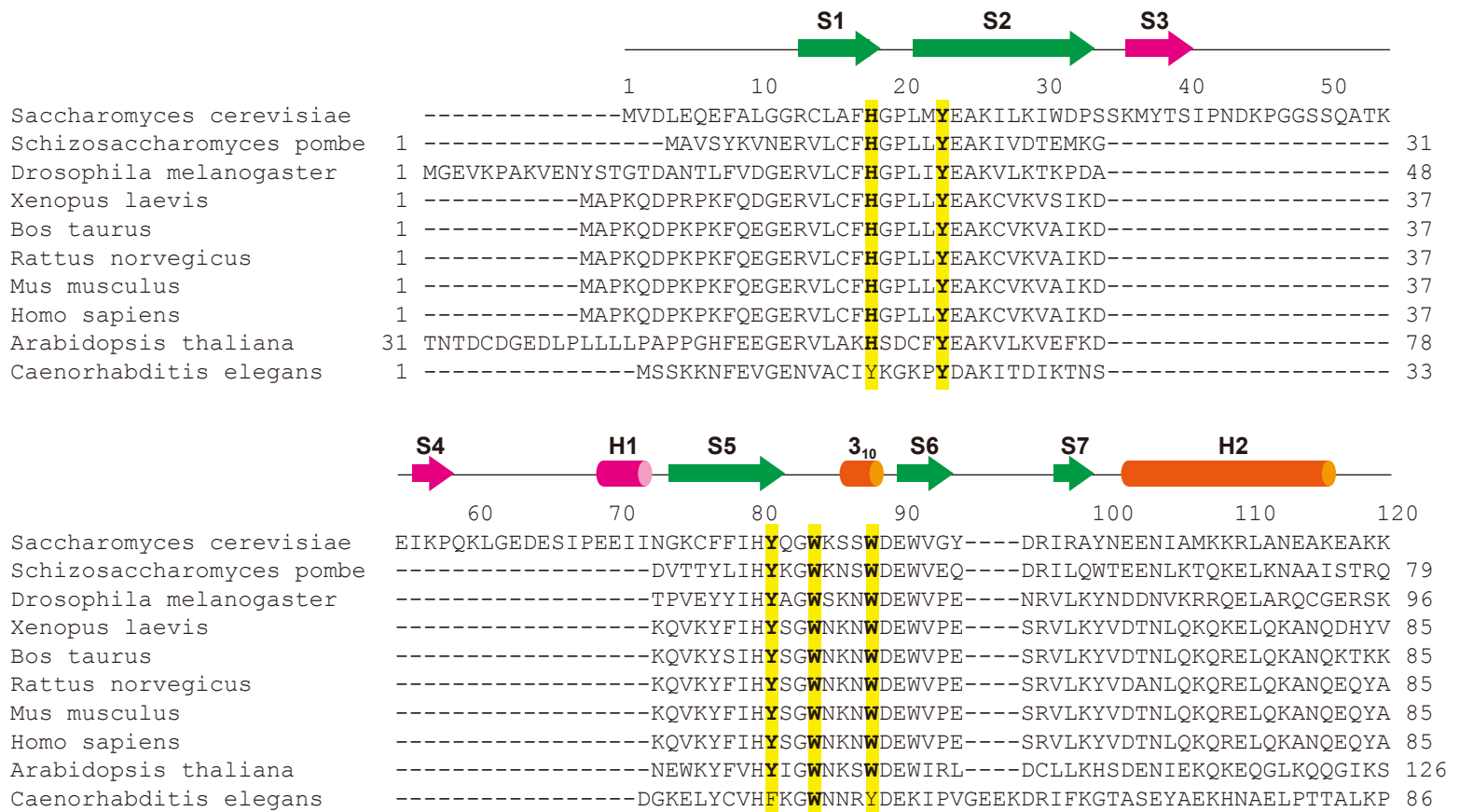


Fig. S5. Sequence alignment of the CD of budding yeast Eaf3 and various homologues. Residues involved in the cage formation are shaded in yellow. The secondary structure of budding yeast Eaf3 CD is shown above the sequence.

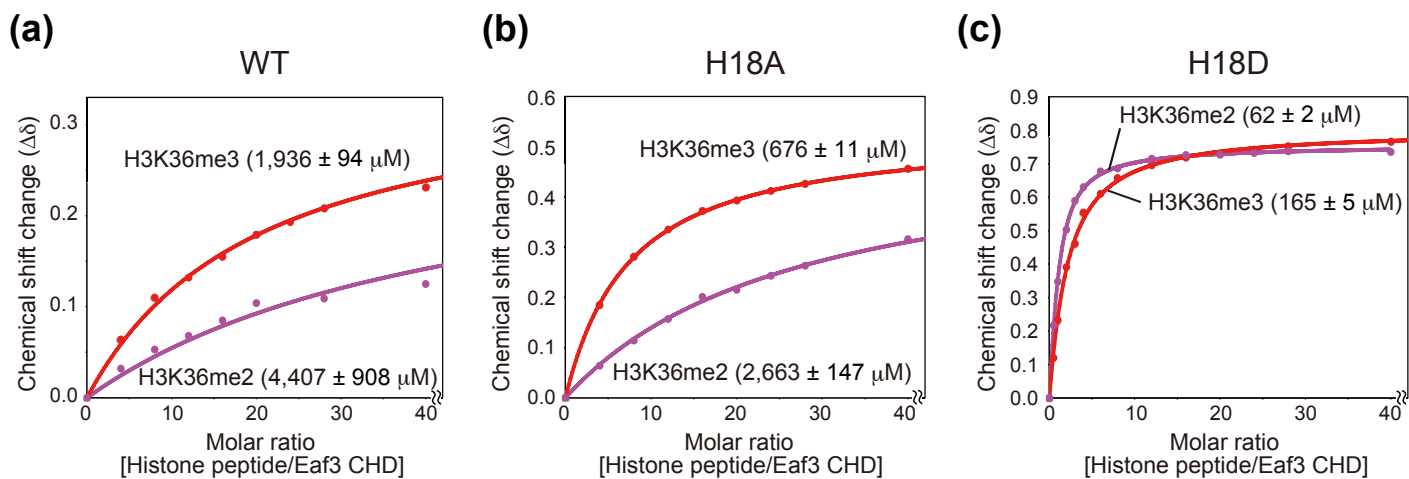


Fig. S6. NMR titration experiment.

Shown are the titration curves for ^{15}N -labeled Eaf3 CD with H3K36me2 and H3K36me3 peptides at pH 6.8. (a) Wild-type Eaf3 CD; (b) H18A mutant; (c) H18D mutant. The titration curves are plotted for Ala25 of Eaf3 CD. Calculated K_d values are given in parentheses.

Table S1. Histone peptides used in the NMR binding experiments

<i>NMR chemical shift perturbation experiment</i>	
Name	Sequence
H3	ARTKQTARKSTGGKAPRKQLASKAARKSAPSTGGVKKPHRYK
H3K4me2	ARTK(me2)QTARKSTGGKAPRKQLASKAARKSAPSTGGVKKPHRYK
H3K36me2	ARTKQTARKSTGGKAPRKQLASKAARKSAPSTGGVK(me2)KPHRYK
H3K4me2K36me2	ARTK(me2)QTARKSTGGKAPRKQLASKAARKSAPSTGGVK(me2)KPHRYK
H3K4	ARTKQTARKSTGGKAPRY
H3K4me2	ARTK(me2)QTARKSTGGKAPRY
H3K9me2	ARTKQTARK(me2)STGGKAPRY
H3K27me2	KQLASKAARK(me2)SAPSTGGVY
H3K36	SAPSTGGVKKPHRYKPGT
H3K36me2	SAPSTGGVK(me2)KPHRYKPGT
H3K79me2	VREIAQDFK(me2)TDLRFQSSY
H4K20me2	KGGAKRHRK(me2)ILRDNIQGY
H3R2ame2	AR(ame2)TKQTARKSTGGKAPRKQLAY
H3R17ame2	ARKSTGGKAPR(ame2)KQLASKAARKY
H3R26ame2	PRKQLASKAAR(ame2)KSAPSTGGVKY
H4R3ame2	SGR(ame2)GKGGKGLGKGGAKRHRKY
H3T3pho	ART(pho)KQTARKSTGGKAPRY
H3K9-23ac	ARK(ac)STGGK(ac)APRK(ac)QLATK(ac)AAY
<i>NMR titration experiment</i>	
H3K4	ARTKQTARKSTGGKAPRY
H3K4me2	ARTK(me2)QTARKSTGGKAPRY
H3K4me3	ARTK(me3)QTARKSTGGKAPRY
H3K36	SAPSTGGVKKPHRYKPGT
H3K36me2	SAPSTGGVK(me2)KPHRYKPGT
H3K36me3	SAPSTGGVK(me3)KPHRYKPGT
H3R2(ame2)K4me3	AR(ame2)TK(me3)QTARKSTGGKAPRY
H3T3(pho)K4me3	ART(ph)K(me3)QTARKSTGGKAPRY

me2: di-methylated, me3: tri-methylated, ame2: asymmetrically di-methylated, pho: phosphorylated, ac: acetylated.

Table S2. Structural statistics for the 20 best structures of Eaf3 CD

Experimental restraints	
Total NOEs	2480
Intraresidue	110
Sequential (i-j =1)	659
Medium-range (1<i-j<5)	546
Intramolecular long-range (i-j≥5)	1165
Hydrogen bond	23 × 2
Number of dihedral restraints	
φ	59
ψ	58
χ1	23
χ2	3
Statistics for structure calculations	
R.m.s.d. from experimental restraints*	
Distance (Å)	0.038 ± 0.001
Dihedral (°)	0.566 ± 0.078
R.m.s.d. from idealized covalent geometry	
Bonds (Å)	0.0060 ± 0.0001
Angles (°)	0.70 ± 0.02
Improper (°)	0.71 ± 0.03
Coordinate precision (residues 7–41, 56–115)	
Average pairwise r.m.s.d. from the mean structure	
Backbone atoms (Å)	0.64 ± 0.12
Heavy atoms (Å)	1.29 ± 0.17
Ramachandran plot statistics (residues 7–41, 56–115)	
Residues in most favored regions (%)	73.8
Residues in additional allowed regions (%)	23.8
Residues in generously allowed regions (%)	2.4
Residues in disallowed regions (%)	0.0

* None of the structures exhibited distance violations of >0.5 Å or dihedral angle violations of >4°.

Table S3. Residues forming the binding site for methyl-lysine residues in the histone tail

Domain	Protein	Histone	PDB ID	Residues having side-chains within 6 Å of N ζ of methylated lysine						
				Aromatic			Charged		Others	
CD	scEaf3	H3K36me2	2K3Y (NMR)	Tyr23	Tyr81	Trp84	Trp88	His18		
	aMRG2	H3K4me3	4PL6 (X-ray)	Tyr67	Tyr87	Trp90	Trp94	His62		
	aMRG2	H3K36me3	4PLI (X-ray)	Tyr67	Tyr87	Trp90	Trp94	His62		
	hMSL3	H4K20me1	3OAE (X-ray)	Tyr31	Phe56	Trp59	Trp63	Glu21		Pro22
	mHP1	H3K9me2	1GUW (NMR)	Tyr21	Trp42	Phe45		Asp49	Glu53	Thr51
	dHP1	H3K9me2	1KNA (X-ray)	Tyr24	Trp45	Tyr48		Glu52		
	dPC	H3K27me3	1PDQ (X-ray)	Tyr26	Trp47	Trp50	Tyr54			Thr56
	dPC	H3K27me3	1PFB (X-ray)	Tyr26	Trp47	Trp50				Thr56
	spChp1	H3K9me3	2RSN (NMR)	Tyr22	Trp44	Tyr47		Asp51		
	spChp1	H3K9me3	3G7L (X-ray)	Tyr22	Trp44	Tyr47		Asp51		
	hCBX1	H3K9me3	6D07 (X-ray)	Tyr3	Trp24	Phe27		Asp31		Thr33
	hCBX2	H3K27me3	3H91 (X-ray)	Phe12	Trp33	Trp36		His40		Ser42
	hCBX3	H3K9me3	2L11 (NMR)	Phe30	Trp51	Phe54		Asp58	Glu62	Thr60
	hCBX3	H1K26me2	3TZD (X-ray)	Phe26	Phe30	Trp51	Phe54	Asp58		
	hCBX5	H3K9me3	3FDT (X-ray)	Tyr20	Trp41	Phe44		His48		Thr50
	hCBX6	H3K9me3	3GV6 (X-ray)	Phe11	Trp32	Trp35	Tyr39			Thr41
	hCBX6	H3K27me3	3GV6 (X-ray)	Phe11	Trp32	Trp35	Tyr39			Thr41
	hCBX7	H3K9me3	2L12 (NMR)	Phe11	Trp32	Trp35				Gln9
	hCBX7	H3K27me3	2L1B (NMR)	Phe11	Trp32	Trp35	Tyr39			Gln9
	mCBX7	H3K27me2	2KVM (NMR)	Phe11	Trp32	Trp35	Tyr39			Thr41
	mCBX7	H3K27me3	4X3K (X-ray)	Phe11	Trp32	Trp35	Tyr39			Thr41
	hCBX8	H3K9me3	3I91 (X-ray)	Phe11	Trp32	Trp35	Tyr39			Thr41
	hCHD1	H3K4me3	2B2W (X-ray)	Trp322	Trp325			Glu272		Thr331
	hMPP8	H3K9me3	3QO2 (X-ray)	Phe59	Trp80	Tyr83		Asp87		
hMPP8	H3K9me3	3R93 (X-ray)	Phe59	Trp80	Tyr83		Asp87			
maZMET2	H3K9me2	4FT2 (X-ray)	Phe441	Trp466	Tyr469		Glu473		Thr475	
dRHINO	H3K9me3	4QUF (X-ray)	Tyr24	Trp45	Phe48				Asn52	
dRHINO	H3K9me3	4U68 (X-ray)	Tyr24	Trp45	Phe48				Asn52	
hCDYL2	H1K26me2	5JJZ (X-ray)	Tyr7	Trp29	Tyr32				Thr38	
PHD	hBPTF	H3K4me3	2FUU (NMR)	Tyr2869	Tyr2876	Tyr2882	Trp2891			
	hING1	H3K4me3	2QIC (X-ray)	Tyr355	Trp378					Ser362
	mING2	H3K4me3	2G6Q (X-ray)	Tyr215	Trp238					Ser222
	hING4	H3K4me3	2PNX (X-ray)	Tyr198	Trp221					Ser205
	hING4	H3K4me3	2VNF (X-ray)	Tyr198	Trp221					Met209
	hING5	H3K4me3	3C6W (X-ray)	Tyr188	Trp211					Ser205
	scYng1	H3K4me3	2JMJ (NMR)	Tyr157	Trp180					Met199
	hTAF3	H3K4me3	5WXH (X-ray)	Trp861	Trp866	Trp889		Asp875		Ser164
	mTAF3	H3K4me3	2K17 (NMR)	Trp868	Trp891			Asp877		Met168
	mRAG2	H3K4me3	2V89 (X-ray)	Tyr415	Trp453					Met880
	hPYGO1	H3K4me2	2VPE (X-ray)	Tyr341	Trp366			Asp352		Met882
	mPYGO	H3K4me3	2YYR (X-ray)	Tyr339	Trp364			Asp350		Gly414
	hPYGO2	H3K4me2	4UP0 (X-ray)	Tyr328	Trp353			Asp339		Met443
	hJARID1A	H3K4me3	3GL6 (X-ray)	Trp1625	Trp1635					Val350
	hPHF2	H3K4me3	3KQI (X-ray)	Tyr7	Tyr14	Trp29				Val348
	hPHF8	H3K4me3	3KV4 (X-ray)	Tyr43	Tyr50	Trp65				Val337
	hPHF13	H3K4me3	3O7A (X-ray)	Phe241	Trp255					Asn338
	hPHF20	H3K4me2	5TBN (NMR)	Trp675				Glu662		Ala343
	hMLL1	H3K4me3	3LQJ (X-ray)	Tyr1576	Tyr1581	Trp1594				Met20
	hMLL5	H3K4me3	4L58 (X-ray)	Trp141				Asp128		Met56
	hDIDO3	H3K4me3	4L7X (X-ray)	Tyr270	Trp291			His277		Ser390
	scSet3	H3K4me3	5TDW (X-ray)	Trp140				Asp127		Ala392
	dPPS	H3K4me3	5WLE (X-ray)	Trp912	Trp933			Asp906	His919	Leu232
	aAL1	H3K4me3	5Y20 (X-ray)	Tyr195	Trp201	Trp210				Met246
aSHL	H3K4me3	5ZNP (X-ray)	Tyr141	Tyr148	Trp163		Asp136		Val653	
Tudor	hJMJD2A	H3K4me3	2GFA (X-ray)	Phe932	Trp967	Tyr973		Asp934		Ser936
	hJMJD2A	H4K29me3	2QQS (X-ray)	Phe932	Trp967	Tyr973		Asp934		Ser936
	h53BP1	H4K20me2	2IG0 (X-ray)	Trp1495	Tyr1502	Phe1519	Tyr1523	Asp1521		
	h53BP1	H4K20me2	2LVM (NMR)	Trp1495	Tyr1502	Phe1519	Tyr1523	Asp1521		
	hUHRF1	H3K9me3	2L3R (NMR)	Phe152	Tyr188	Tyr191	Phe237	Asp145		Asn194
	hUHRF1	H3K9me3	3ASK (X-ray)	Phe152	Tyr188	Tyr191		Asp145		Asn194
	hUHRF1	H3K9me3	3DB3 (X-ray)	Phe152	Tyr188	Tyr191		Asp145		Asn194
	hUHRF1	H3K9me3	4GY5 (X-ray)	Phe152	Tyr188	Tyr191		Asp145		Asn194
	hSGF29	H3K4me3	3MEA (X-ray)	Tyr238	Tyr245	Phe264		Asp266		
	hSPINDLIN1	H3K4me3	4H75 (X-ray)	Phe141	Trp151	Tyr170	Tyr177	Tyr179	Asp173	
	hSPINDLIN1	H4K20me3	5Y5W (X-ray)	Phe141	Trp151	Tyr170	Tyr177	Tyr179	Asp173	
	hSPINDLIN4	H3K4me3	4UY4 (X-ray)	Phe127	Trp137	Tyr156	Tyr163	Tyr165	Asp159	

Table S3. Residues forming the binding site for methyl-lysine residues in the histone tail

Domain	Protein	Histone	PDB ID	Residues having side-chains within 6 Å of Nζ of methylated lysine						
				Aromatic			Charged		Others	
Tudor	hPHF1	H3K36me3	2M0O (NMR)	Tyr47	Phe65				Asp67	Ser69
	hPHF1	H3K36me3	4HCZ (X-ray)	Trp41	Tyr47	Phe65	Phe71		Asp67	Ser69
	aSHH1	H3K9me3	4IUR (X-ray)	Tyr140	Phe162	Phe165			Asp136 His169 Glu171	Ser133
	hPHF19	H3K36me3	4BD3 (NMR)	Trp50	Tyr56	Phe74	Tyr80		Asp76	Ser78
MBT	hL3MBTL1	H4K20me2	2PQWI (X-ray)	Phe379	Trp382	Tyr386			Asp355	Asn358 Leu361 Cys363 Thr411
	hL3MBTL1	H1.5K27me2	2RHI (X-ray)	Phe379	Trp382	Tyr386			Asp355	Asn358 Leu361 Cys363 Thr411
	hL3MBTL2	H4K20me1	3F70 (X-ray)	Phe570	Trp573	Tyr577			Asp546	Leu552 Cys554
	dSCM	Kme	2R5A (X-ray)	Phe348	Trp351	Phe355			Asp324	Asn327 Leu330 Cys332 Gln380
	hSCML2	Kme	2VYT (X-ray)	Phe206	Trp209	Phe213			Asp182	Asn185 Leu188 Cys190
PWWP	hBRPF1	H3K36me3	2X4W (X-ray)	Tyr1096	Tyr1099	Phe1147			Asp1149	Cys1093 Thr1153
	hZFCW	H3K4me3	2RR4 (NMR)	Trp256	Trp267	Trp303				
	hHDGF2	H3K79me3	3QJ6 (X-ray)	Tyr18	Trp21	Phe44			Glu49	Met15 Thr47
	mZMYND11	H3K36me3	4N4H (X-ray)	Phe291	Trp294	Phe310				Met288 Gln316
	hZCWPW2	H3K4me3	4O62 (X-ray)	Trp30	Trp41	Phe78				
	hDNMT3B	H3K36me3	5CIU (X-ray)	Phe236	Trp239	Trp263			Asp266	Ile233
	mMORC3	H3K4me3	5IX1 (X-ray)	Trp410	Trp419				Glu450 Glu453	
	hMORC3	H3K4me3	5SVX (X-ray)	Trp410	Trp419				Glu450 Glu453	
	hHRP3	H3K36me3	6IIS (X-ray)	Tyr23	Trp26	Phe49			Glu54	Met20 Thr52
	WD40	hEED	H1K26me3	3Ily (X-ray)	Phe97	Tyr148	Trp364	Tyr365		
hEED		H3K9me3	3IJ0 (X-ray)	Phe97	Tyr148	Trp364	Tyr365			Asn194
hEED		H3K27me3	3IIW (X-ray)	Phe97	Tyr148	Trp364	Tyr365			Asn194
hEED		H4K20me3	3IJ1 (X-ray)	Phe97	Tyr148	Trp364	Tyr365			Asn194
hEED		H3K27me3	3JZG (X-ray)	Phe97	Tyr148	Trp364	Tyr365			Asn194
hEED		H3K79me3	3JZH (X-ray)	Phe97	Tyr148	Trp364	Tyr365			Asn194
hEED		H3K4me3	3K26 (X-ray)	Phe97	Tyr148	Trp364	Tyr365			Asn194
hEED		H3K9me3	3K27 (X-ray)	Phe97	Tyr148	Trp364	Tyr365			Asn194
BAH	mORC1	H4K20me2	4DOW (X-ray)	Tyr63	Trp87	Tyr114	Trp119		Glu93	Val89
	maZMET2	H3K9me2	4FT4 (X-ray)	Tyr203	Trp224	Phe226			Asp230	
	aSHL	H3K27me3	5ZNR (X-ray)	Tyr41	Trp63	Tyr65			Glu69 His88	
Ankyrin	hGLP	H3K9me2	3B95 (X-ray)	Trp874	Trp879	Tyr883	Trp912		Glu882	Ile878
ADD	hATRX	H3K9me3	2LBM (NMR)	Tyr203					Asp207 Glu225	Ile209 Gln219 Ala224
	hATRX	H3K9me3	3QL9 (X-ray)	Tyr203					Asp207 Glu225	Ser206 Ile209 Gln219 Ala224

h : *Homo sapiens*,
m : *Mus musculus*,
d : *Drosophila melanogaster*,
sp : *Schizosaccharomyces pombe*,
sc : *Saccharomyces cerevisiae*,
a : *Arabidopsis thaliana*,
ma : *Zea mays*

Table S4. Residues of Eaf3 CD in which the side-chains are within 6 Å of Nζ of the H3K36me2 analog bound to Eaf3 CD

Residue	Atom	Distance (Å)
18 HIS	Cγ	5.525
18 HIS	Nδ1	5.432
18 HIS	Cδ2	5.091
18 HIS	Cε1	4.888
18 HIS	Nε2	4.655
<hr/>		
23 TYR	Cβ	4.789
23 TYR	Cγ	4.128
23 TYR	Cδ1	4.860
23 TYR	Cδ2	3.365
23 TYR	Cε1	4.952
23 TYR	Cε2	3.474
23 TYR	Cζ	4.341
23 TYR	Oζ	5.061
<hr/>		
81 TYR	Cβ	4.894
81 TYR	Cγ	4.539
81 TYR	Cδ1	4.336
81 TYR	Cδ2	5.023
81 TYR	Cε1	4.615
81 TYR	Cε2	5.283
81 TYR	Cζ	5.112
81 TYR	Oζ	5.906
<hr/>		
84 TRP	Cβ	4.914
84 TRP	Cγ	4.420
84 TRP	Cδ1	4.201
84 TRP	Cδ2	4.489
84 TRP	Nε1	3.974
84 TRP	Cε2	4.135
84 TRP	Cε3	5.211
84 TRP	Cζ2	4.537
84 TRP	Cζ3	5.617
84 TRP	Cη2	5.317
<hr/>		
88 TRP	Cβ	4.850
88 TRP	Cγ	4.287
88 TRP	Cδ1	4.495
88 TRP	Cδ2	4.081
88 TRP	Nε1	4.444
88 TRP	Cε2	4.164
88 TRP	Cε3	4.410
88 TRP	Cζ2	4.504
88 TRP	Cζ3	4.749
88 TRP	Cη2	4.792